Received: 10 November 2020 | Accepted: 14 November 2020

DOI: 10.1002/jnr.24760

RESEARCH ARTICLE

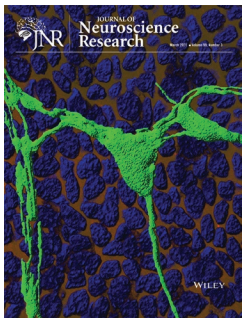

Graph theory analysis of the dopamine D2 receptor network in Parkinson's disease patients with cognitive decline

Alexander S. Mihaescu[1,2,3] | Jinhee Kim[1] | Mario Masellis[3,4,5] | Ariel Graff-Guerrero[1,3] | Sang Soo Cho[2] | Leigh Christopher[1] | Mikaeel Valli[1,2,3] | María Díez-Cirarda[1,2,6] | Yuko Koshimori[1] | Antonio P. Strafella[1,2,3,7]

[1]Research Imaging Centre, Campbell Family Mental Health Research Institute, Centre for Addiction and Mental Health, University of Toronto, Toronto, ON, Canada

[2]Division of Brain, Imaging and Behaviour – Systems Neuroscience, Krembil Research Institute, University Health Network, University of Toronto, Toronto, ON, Canada

[3]Institute of Medical Science, University of Toronto, ON, Canada

[4]LC Campbell Cognitive Neurology Research Unit, Sunnybrook Research Institute, University of Toronto, Toronto, ON, Canada

[5]Hurvitz Brain Sciences Program, Sunnybrook Research Institute, Toronto, ON, Canada

[6]Neurodegenerative Diseases Group, Biocruces Bizkaia Health Research Institute, Barakaldo, Spain

[7]Morton and Gloria Shulman Movement Disorder Unit & E.J. Safra Program in Parkinson Disease, Neurology Division, Department of Medicine, Toronto Western Hospital, University Health Network, University of Toronto, Toronto, ON, Canada

Correspondence
Alexander S. Mihaescu and Antonio P. Strafella, Research Imaging Centre, Campbell Family Mental Health Research Institute, Centre for Addiction and Mental Health, University of Toronto, Toronto, ON, Canada.
Email: alex.mihaescu@alum.utoronto.ca (A. S. M.) and antonio.strafella@uhnres.utoronto.ca (A. P. S.)

Funding information
Canadian Institutes of Health Research

Abstract

Cognitive decline in Parkinson's disease (PD) is a common sequela of the disorder that has a large impact on patient well-being. Its physiological etiology, however, remains elusive. Our study used graph theory analysis to investigate the large-scale topological patterns of the extrastriatal dopamine D2 receptor network. We used positron emission tomography with [^{11}C]FLB-457 to measure the binding potential of cortical dopamine D2 receptors in two networks: the meso-cortical dopamine network and the meso-limbic dopamine network. We also investigated the application of partial volume effect correction (PVEC) in conjunction with graph theory analysis. Three groups were investigated in this study divided according to their cognitive status as measured by the Montreal Cognitive Assessment score, with a score ≤25 considered cognitively impaired: (a) healthy controls (n = 13, 11 female), (b) cognitively unimpaired PD patients (PD-CU, n = 13, 5 female), and (c) PD patients with mild cognitive impairment (PD-MCI, n = 17, 4 female). In the meso-cortical network, we observed increased small-worldness, normalized clustering, and local efficiency in the PD-CU group compared to the PD-MCI group, as well as a hub shift in the PD-MCI group. Compensatory reorganization of the meso-cortical dopamine D2 receptor network may be responsible for some of the cognitive preservation observed in PD-CU. These results were found without PVEC applied and PVEC proved detrimental to the graph theory analysis. Overall, our findings demonstrate how graph theory analysis can be used to detect subtle changes in the brain that would otherwise be missed by regional comparisons of receptor density.

KEYWORDS

[^{11}C]FLB-457, cognitive decline, dopamine D2 receptors, graph theory, Parkinson's disease, partial volume effect correction

Edited by Lerner Talia. Reviewed by David Eidelberg.

1 | INTRODUCTION

Parkinson's disease (PD) is the second most common neurodegenerative disorder after Alzheimer's disease (AD), with a complex etiology involving progressive motor and cognitive impairments (De Lau & Breteler, 2006; Hirsch et al., 2016). Cognitive decline in PD affects between 20% and 50% of PD patients, however, its neurological etiology remains elusive (Aarsland et al., 2017; Goldman & Litvan, 2011). Loss of dopamine producing neurons in the substantia nigra is a driving force behind the motor symptoms (Jankovic, 2008), but dysfunctional dopaminergic activity in the cerebrum is also thought to have an important role in PD cognitive decline (Bellucci et al., 2016; Chaudhuri & Schapira, 2009; Chung et al., 2018; Ito et al., 2002; Jokinen et al., 2009; Rinne et al., 2000).

Cognitive decline in PD occurs along a spectrum, beginning with patients who are cognitively unimpaired (PD-CU), then ranging to mild cognitive impairment (PD-MCI) and finally PD dementia (Litvan et al., 2012). [^{11}C]FLB-457 is a high-affinity radiotracer for measuring extrastriatal dopamine D2 receptor (D2R) density (Halldin et al., 1995) and the D2R system has been frequently studied for its role in PD neuropathology (Christopher et al., 2014; Ko et al., 2013). Using [^{11}C]FLB-457, Christopher and colleagues (2014) found that PD-MCI patients have decreased D2R availability in the bilateral insula compared to PD-CU patients and healthy controls (HC), with the insula being an important associative hub for coordinating relevant information from multiple cognitive domains. Furthermore, insular D2R levels predicted executive function in this study, with lower D2R availability in the insula also resulting in poorer executive test scores. The dopaminergic networks dysregulated by PD (McCutcheon et al., 2019; Premi et al., 2016) suggest that PD pathology may be described as a disconnection syndrome (Caminiti, Presotto, et al., 2017; Cronin-Golomb, 2010).

New studies have begun to go beyond measuring regional increases or decreases in radioligand binding, and instead focus on the differences in whole-brain network communication patterns as a potential source for the subtle and difficult to pin-down cognitive decline in PD (Baggio et al., 2014; Luo et al., 2015). Since the beginning of the application of graph theoretical approaches to brain networks over 10 years ago, numerous studies have found changes in common brain networks in PD patients as measured by resting-state functional magnetic resonance imaging (fMRI) (Díez-Cirarda et al., 2018; Göttlich et al., 2013; Kim et al., 2017; Putcha et al., 2015). Graph theory analysis allows us to investigate the topological architecture of human brain networks (Bullmore & Sporns, 2009). Previous studies have shown that the brain as a large-scale network exhibited small-world properties which is characterized by a balance between segregation (i.e., specialized processing) and integration (i.e., whole-brain transfers) of information (Bressler, 1995; Rubinov & Sporns, 2010; Sporns, 2011; Van Den Heuvel & Pol, 2010). The two basic units in a graph are nodes (being specific areas of the brain) and edges (representing the relationship between two nodes) (Bullmore & Sporns, 2009). Random graphs tend to minimize path length between nodes while ordered lattice graphs tend to maximize clustering (Telesford et al., 2011). Small-world topology is a "Goldilocks" balance where the graph is not too ordered (resulting in long paths between distant brain regions) and not too random (resulting in long path length between neighboring nodes sharing a similar function) (Bassett & Bullmore, 2006).

Significance

It is not currently well understood why some Parkinson's disease (PD) patients experience progressive cognitive decline while others do not. In this study, we applied graph theory analysis on positron emission tomography imaging data to characterize the complex patterns of the dopamine D2 receptor system in PD patients. We found that cognitively unimpaired PD patients had more efficient information flow in the meso-cortical network compared to PD patients with mild cognitive impairment. This is the first study to apply graph theory analysis to a dopamine receptor network and suggests the utility of applying this methodology to other neuroreceptor systems.

The application of graph theory analysis to positron emission tomography (PET) imaging data began with a focus on the radiotracers Pittsburgh compound B and [^{18}F] Fluoro-2-deoxy-D-glucose (FDG), which are radiotracers that measure beta-amyloid plaque density and brain glucose activity, respectively (Kim et al., 2019; Verger et al., 2018). The extension of this method to radiotracers that measure neuroreceptors occurred within the last few years (Ashok et al., 2019; Caminiti, Presotto, et al., 2017; Veronese et al., 2019), and there is no current gold standard for the theoretical and practical methodologies involved in neuroreceptor graph theory analyses. In PET graph theory analysis, relationships between different brain regions are calculated as inter-regional statistical correlations in the intensity values (i.e., radioligand density measure) across subjects in each group.

Fazio and colleagues (2020) performed a graph theory analysis of a neuroreceptor system, examining the serotonin transporter (SERT) network in a 2-year longitudinal study between HC and PD patients. While no differences were found between the groups at baseline, in the follow-up, PD patients had reduced global efficiency and increased transitivity compared to HC. Global efficiency is a measure of how well the brain can send information over the entire network while transitivity is how closely small clusters form connections with their neighbors (Latora & Marchiori, 2001). Interestingly, there were no differences observed between the PD and HC in regional SERT levels, or any regional SERT differences between the baseline and follow-up in PD patients, suggesting the utility of the graph theory analysis' ability to detect subtle changes that would otherwise be missed through regional comparisons.

It has been known for over 20 years that the dopamine D2R networks are linked intimately to cognition and affect the executive function and attentional networks in healthy subjects (Volkow

et al., 1998). However, there is still much debate on how the D2R network is involved in cognition. One hypothesis is that the D2R is involved in facilitating cognitive flexibility (Christopher et al., 2014; Floresco & Magyar, 2006; van Holstein et al., 2011). Much of the research on extrastriatal dopamine physiology has focused on the frontal cortex. Another, newer hypothesis, however, is that the D2R system is instead involved in hippocampus-based cognition through striatal and hippocampal signaling (Nyberg et al., 2016). Our study will attempt to tease apart these findings by dividing the cortical dopamine system into two smaller subnetworks: the meso-cortical pathway projecting to the prefrontal and dorsolateral frontal regions and the meso-limbic pathway projecting to the ventral and medial frontal areas along with other limbic regions (Caminiti, Tettamanti, et al., 2017; Oades & Halliday, 1987; Tziortzi et al., 2014).

The aim of our study was to explore a novel method of analyzing PET data using graph theory analysis. We measured cortical D2R density using the radiotracer [^{11}C]FLB-457 (Halldin et al., 1995). To our knowledge, no study has been performed on the network topological properties of the D2R network, in HC or in PD patients. We investigated if there were any differences in network topology in the dopamine D2R networks between three groups: HC, PD-CU, and PD-MCI. We hypothesize PD-MCI patients will have less flexible and efficient flow in their D2R networks compared to PD-CU patients. Previous studies have suggested age-related gray matter atrophy can lead to an underestimation of the radioligand signal and partial volume effect correction (PVEC) should be applied to reduce the effect of age-related differences and increase D2R radioligand signal (Morris et al., 1999; Smith et al., 2019). This paper will present two different methods of analyzing the D2R network, both with and without PVEC applied, as an exploratory demonstration of the utility in applying graph theoretical methods to other pre-existing PET neuroreceptor data sets while discussing the advantages and shortcomings of each method.

2 | MATERIALS AND METHODS

2.1 | Participants and study design

A total of 43 participants were included in this imaging analysis: 30 patients with PD (mean age 69.37 years ± 6.13, 9 female) and 13 age-similar HC (mean age 66.0 years ± 4.18, 11 female). Participants ranged in age from 58 to 80 and were matched for age within 5 years. Imaging data from some of these participants were reported previously in a prior study (Christopher et al., 2014). All PD patients met the UK Parkinson's disease Society Brain Bank Criteria. Potential participants were excluded if they had any other neurological or psychiatric conditions, or if they met the criteria for PD with dementia classification (Emre et al., 2007) as measured by a clinical neurologist, Dr. Antonio Strafella. The 30 PD patients were divided into two groups: 13 PD patients were classified as PD-CU (mean age 67.62 years ± 5.68, 5 female) while 17 PD patients were classified as PD-MCI (mean age 70.71 ± 6.28, 4 female). PD patients in the two groups were matched based on disease severity with the Unified Parkinson's Disease Rating Scale Part III and levodopa equivalent daily dose (LEDD). The 13 HC participants had no history of any neurological or psychiatric conditions and no evidence of any cognitive impairment at the time of testing as assessed by a neurocognitive test battery and the Montreal Cognitive Assessment (MoCA) (Nasreddine et al., 2005). All participants were also matched based on their estimated premorbid IQ score measured by the Wechsler Test of Adult Reading (Wechsler, 1997) and were screened for depression using the Beck's Depression Inventory (Beck et al., 1961). Demographic and clinical information is presented in Table 1. Neuropsychological testing was performed with PD patients ON medication. LEDD is based on the theoretical equivalence of various drugs to L-DOPA and was calculated based on previous studies (Evans et al., 2004; Parkin et al., 2002). PD patients were scanned OFF medication after an overnight 12-hr withdrawal from their antiparkinsonian medication. This is done to minimize the effect of antiparkinsonian medication on the scans while maintaining patient comfort and functioning (Defer et al., 1999). All participants were scanned with the radiotracer [^{11}C]FLB-457 which binds with high affinity to extrastriatal dopamine D2R. This radiotracer can be used to quantify postsynaptic D2R binding in cortical regions of the brain but cannot accurately quantify striatal D2R density. All participants provided informed, written consent prior to beginning the study procedures and this study was approved by the research ethics committees for the Centre for Addiction and Mental Health, the University Health Network and in compliance with the Declaration of Helsinki (Christopher et al., 2014).

2.2 | Magnetic resonance imaging (MRI) data acquisition

All participants underwent an MRI scan to obtain a high-resolution T1-weighted structural MRI scan which was used to coregister the PET images. Structural MRI data were collected using a 3T GE Discovery MR 750 scanner with an 8-channel radio frequency head coil. T1-weighted high-resolution data were obtained for functional overlay using a fast-spoiled gradient echo pulse sequence with the following parameters: repetition time = 6.7 ms; echo time = 3.0 ms; flip angle = 8°; field of view = 230 × 230 mm^2; matrix size = 256 × 256 × 200; sagittal slices; and voxel size = 0.89 × 0.89 × 0.9 mm^3.

2.3 | Neuropsychological assessment of cognitive status

The PD patients included in the study were classified as PD-MCI according to their score on the MoCA. PD patients were categorized as PD-CU if they scored 26 or higher on the MoCA, or else they were categorized as PD-MCI if they scored 25 or lower on the MoCA. The Movement Disorders Society Task Force found that the

TABLE 1 Demographics, clinical information, and PET radiotracer parameters of the healthy controls and Parkinson's disease patients

Group	HC ($n = 13$)	PD-CU ($n = 13$)	PD-MCI ($n = 17$)	PD Total ($n = 30$)
Sex [female, male]	11F, 2M	5F, 8M	4F, 13M	9F, 21M[c]
Age (years)	66.0 ± 4.18	67.62 ± 5.68	70.71 ± 6.28	69.37 ± 6.13
Education (years)	17.38 ± 2.29	15.92 ± 2.93	16.29 ± 2.08	16.13 ± 2.08
MoCA	28.31 ± 1.25	27.15 ± 1.14	22.29 ± 2.34[a,b]	24.40 ± 3.09
BDI	2.0 ± 1.0	4.08 ± 2.93	3.94 ± 3.67	4 ± 3.31
Disease duration (years)	n/a	7.5 ± 4.73	6.59 ± 3.52	6.98 ± 4.04
UPDRS-III	n/a	21.92 ± 11.27	26.53 ± 10.59	24.53 ± 10.95
H&Y	n/a	2.04 ± 0.32	2.27 ± 0.44	2.167 ± 0.4
LEDD (mg)	n/a	830.26 ± 528.11	622.58 ± 396.58	712.58 ± 461.67
Injected doses (mCi)	9.80 ± 0.71	9.50 ± 0.63	9.77 ± 0.53	9.66 ± 0.58
Specific activity (mCi/μmol)	3,211.89 ± 1,961.71	3,489.31 ± 1,334.23	3,731.45 ± 1,566.63	3,626.52 ± 1,451.08
Injected mass (μg)	1.68 ± 1.11	1.14 ± 0.41	1.12 ± 0.47	1.13 ± 0.44

Note: Mean ± standard deviation. Statistical significance was determined by a one-way between subjects ANOVA for age, education, MoCA, BDI, disease duration, UPDRS-III score, LEDD, injected doses, specific activity and injected mass, a Kruskal–Wallis H test for Hoehn and Yahr score, and a chi-square test for gender difference.

Abbreviations: BDI, Beck's Depression Inventory; F, female; H&Y, Hoehn and Yahr staging; HC, healthy controls; LEDD, levodopa equivalent daily dose; M, male; MoCA, Montreal Cognitive Assessment; PD-CU, cognitively unimpaired Parkinson's disease patients; PD-MCI, Parkinson's disease patients with mild cognitive impairment; UPDRS-III, Unified Parkinson's Disease Rating Scale – part 3.

[a]Difference found between PD-MCI and PD-CU at $p < 0.05$ using a one-way between subjects ANOVA post-hoc Tukey test ($p < 0.001$)

[b]Difference found between PD-MCI and HC at $p < 0.05$ using a one-way between subjects ANOVA post-hoc Tukey test ($p < 0.001$)

[c]Difference found between the three groups at $p < 0.05$ using a chi-square test.

MoCA is sufficient for Level 1 categorization of PD-MCI patients, which is a diagnostic category of PD-MCI without further PD subtype classification (Dalrymple-Alford et al., 2010; Gill et al., 2008). A MoCA score ≤25 is a suitable cut-off point for PD-MCI classification with good sensitivity and specificity (Dalrymple-Alford et al., 2010; Hoops et al., 2009) and PD patients with dementia were excluded in the initial screening. All HC had a MoCA score of 26 or higher.

2.4 | PET data acquisition

The [^{11}C]FLB-457 scans were performed at the Centre for Addiction and Mental Health using a high-resolution research tomograph scanner (HRRT; Siemens) which measures brain radioactivity in 207 sections with a thickness of 1.22 mm for each slice. The detectors of the HRRT are an LSO/LYSO phoswich detector which has a detection crystal element measuring $2 \times 2 \times 10$ mm^3. A 10-min transmission scan was first performed to correct the PET images for attenuation using a single photon point source, cesium 137 (half-life: 30.2 years, energy: 662 keV). Next, custom-made thermoplastic facemasks and a head-fixation system (Tru-Scan Imaging) were used to minimize participants' head movement while scanning. An average of 9.70 ± 0.62 mCi of [^{11}C]FLB-457 was injected as a bolus into an intravenous line placed in an antecubital vein. PET imaging data were acquired over 90 min while participants were awake and at rest. PET images were reconstructed using a filtered back-projection algorithm, with a Hann filter at Nyquist cut-off frequency. The PET images were reconstructed into 31 frames consisting of 1 background frame (between 44 and 372 s), 15 × 60 s frames, and 15 × 300 s frames.

2.5 | PET image preprocessing

We preprocessed the PET data using two methods: the first method created a voxel-based non-displaceable binding potential (BP_{ND}) map without partial volume effect correction (no-PVEC) and the second method was a region of interest (ROI)-based method that applied PVEC. Both methods estimated the BP_{ND} using the time activity curves (TAC) with the cerebellum as a reference region (Figure 1) which has been deemed suitable as a reference region for the calculation of [^{11}C]FLB-457 BP_{ND} in several studies (Ito et al., 2001; Narendran et al., 2011; Olsson et al., 2004). BP_{ND} is the specific to non-specific partition coefficient calculated such that $BP_{ND} \propto B_{max}/K_D$ where B_{max} is D2R density and $1/K_D$ is the *in vivo* affinity of [^{11}C]FLB-457 to D2R (Seeman & Madras, 2013; Swerdlow, 2010). Applying PVEC to [^{11}C]FLB-457 data has been suggested to be useful in reducing the effect of age-related differences in BP_{ND} due to gray matter atrophy and PVEC increases the estimated BP_{ND} in general (Smith et al., 2019). The present study investigated how PVEC would affect the BP_{ND} when used in conjunction with graph theory methodology.

The voxel-based, no-PVEC method was performed using ROMI (version 2.2017), an in-house automated PET processing

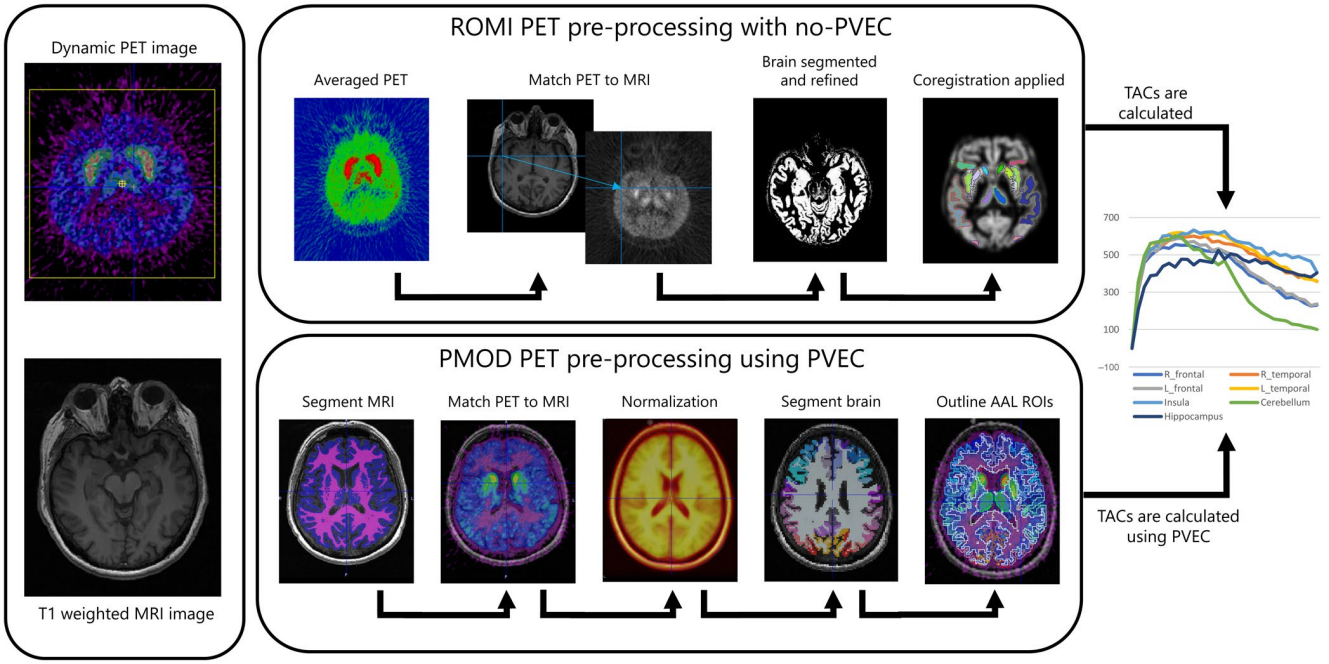

FIGURE 1 Preprocessing begins for both methodologies with a dynamic positron emission tomography (PET) image and a T1-weighted magnetic resonance imaging (MRI) image shown in the left panel. The top panel shows the ROMI pipeline without partial volume effect correction (PVEC) which starts by creating an average PET image for each participant. This averaged PET image is then coregistered with the MRI image using a normalized mutual information coregistration implemented in SPM2. Next, the brain is segmented into gray matter, white matter, and cerebrospinal fluid. A non-linear transformation is applied to a standardized brain template (Montreal Neurological Institute MNI template ICBM/MNI 152 PD brain) to fit each person's MRI image using an automated feature matching algorithm. This template is then refined, which uses a gray matter probability of voxels to account for inter-subject brain variations, and the coregistration is then applied. In the bottom panel, the PMOD PNEURO pipeline using PVEC is shown. This preprocessing pipeline starts by segmenting the MRI images into gray matter, white matter, and cerebrospinal fluid. The PET images are rigidly matched to their corresponding MRI image and then normalized. After normalization, the PET, MRI and atlas images can all be reversibly mapped to each other. The MRI image is then fused with the transformed atlas so that each pixel can be mapped to an area in the atlas. The transformed, fused MRI with pixelwise atlas labeling is then outlined on the PET image. The time activity curves (TACs) are extracted at the end of both pipelines which are used to calculate the non-displaceable binding potentials for each participant, with PVEC applied just before creating the TACs in the PMOD method [Color figure can be viewed at wileyonlinelibrary.com]

software, as well as Statistical Parametric Mapping software (SPM 8; Wellcome Department of Imaging Neuroscience, London, UK). This validated image processing pipeline (Rusjan et al., 2006) is summarized below. First, a non-linear transformation was applied to a standardized brain template (Montreal Neurological Institute MNI template ICBM/MNI 152 PD brain) to transform each participant's T1 MRI image to standardized stereotaxic space using an automated feature matching algorithm. The ROIs from this transformed template were then refined using gray matter probability of voxels from each individual's MRI image to account for inter-subject variability in ROI matching. PET images were then realigned and coregistered to their corresponding MRI image, transforming them to standardized stereotaxic space and TACs were then extracted. Using these TACs, voxel-based parametric BP_{ND} images were created for each participant using Receptor Parametric Mapping (RPM; Gunn et al., 1997) and SPM12 on MATLAB. We used the simplified reference tissue model (SRTM) with the cerebellum as a reference region, as delineated by the ROMI atlas (Lammertsma & Hume, 1996) to calculate these BP_{ND} images. The SRTM has been shown to provide an accurate calculation of BP_{ND} using [^{11}C]FLB-457 without needing an arterial input (Sandiego et al., 2015). These BP_{ND} images were then smoothed, realigned, and registered to the corresponding MRI (Woods et al., 1993) and then transformed to stereotaxic space (Talairach & Tournoux, 1988). All PET images were smoothed with an arbitrary isotropic Gaussian 6 mm full-width half-maximum to homogenize some of the inter-subject PET variability. The Automated Anatomical Labeling (AAL) atlas was then used to parcellate the BP_{ND} images into ROIs and we extracted the BP_{ND} of each ROI using Graph Analysis Toolbox (GAT) for graph theory analysis (Tzourio-Mazoyer et al., 2002). We used age as a covariate for the no-PVEC analysis to minimize factors affecting the network metrics.

The PET data were also preprocessed a second time to apply PVEC on the imaging data set. This was performed using the PMOD PNEURO (version 4.05) and PKIN (version 3.8) software packages. The Müller–Gärtner method of PVEC was performed to account for brain matter volume loss due to aging affecting the recovery of the PET signal (Müller-Gärtner et al., 1992). The same AAL atlas previously used in the no-PVEC method was used for the PVEC ROI parcellation as well. The PMOD pipeline begins by inputting the T1 MRI and PET images, cropping them, then segmenting the MRI image into

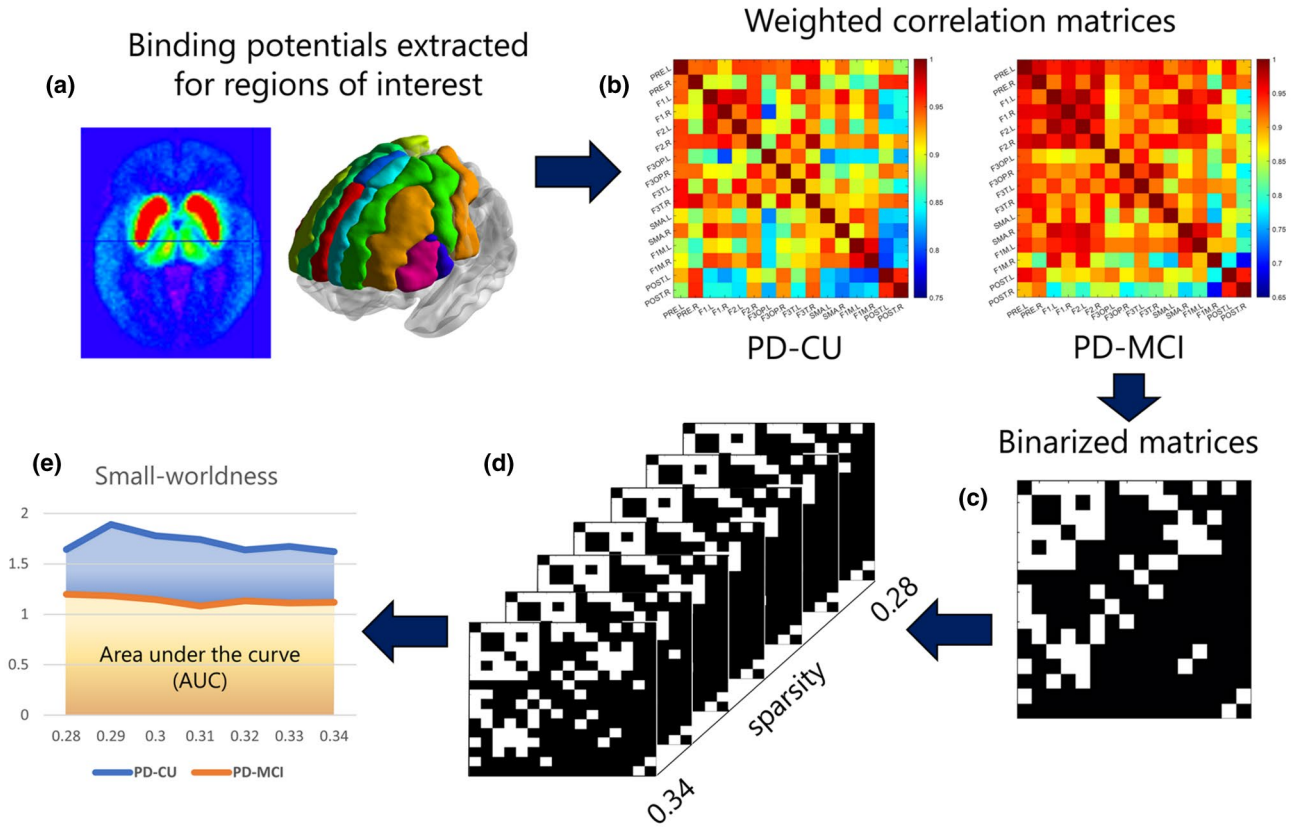

FIGURE 2 This is a graphical representation of the Graph Analysis Toolbox (GAT) processing steps. (a) The non-displaceable binding potentials for each participant in a group is extracted using GAT for each region of interest (ROI) in the included network, shown here for the meso-cortical network constructed using the Automated Anatomical Labeling (AAL) atlas. (b) This creates a group level weighted correlation coefficient matrix which shows the relationships between different ROIs. (c) These weighted matrices are binarized at a certain sparsity threshold 0.*n*. This is achieved by assigning a 1 to the strongest *n*% of correlation coefficients, making those cells a white square that signifies a relationship exists between those two ROIs in that cell. A 0 is assigned otherwise making the cell a black square signifying no relationship exists between those two ROIs. (d) These binarized matrices are calculated across a sparsity threshold, from minimum density (in this example 0.28 where the top 28% of cells are white) to maximum density of 0.34, increasing stepwise by 0.01. (e) Using these binarized matrices, area under the curve (AUC) values are calculated for each topological measure, which can be tested for statistical significance between groups. In this figure, the graph shows the small-worldness index across sparsity values 0.28 to 0.34 for the meso-cortical network comparing cognitively unimpaired Parkinson's disease group (PD-CU) with the Parkinson's disease with mild cognitive impairment group (PD-MCI) [Color figure can be viewed at wileyonlinelibrary.com]

gray matter, white matter, and cerebrospinal fluid. The average PET image is then rigidly matched to the corresponding MRI image. The subjects' images are normalized using the previously calculated MRI segments so that the atlas, MRI, and PET images can be mapped to each other interchangeably. The transformed atlas is then fused with the MRI image pixel by pixel and the atlas's ROI structures are then outlined and applied to the PET images. The PVEC algorithm is then applied at this step before the final TACs are calculated and saved. The 18 AAL ROIs for the cerebellum were combined to create a cerebellum reference region which was used to extract the TACs. The TACs were then kinetically modeled in PKIN using Simplified Reference Tissue Model 2 (SRTM2) to obtain the BP_{ND} of each ROI. SRTM2 was used because SRTM produced BP_{ND} values that were erroneously too high in the frontal lobe for a few subjects (BP_{ND} calculated as 20.0, the maximum BP_{ND} set by default in the PMOD software). This was likely due to the low BP_{ND} in some of these regions, resulting in a noisier BP_{ND} image as the software struggles to find the very small k_2 for these pixels. SRTM and SRTM2 otherwise have excellent agreement with each other overall for a 90 min scan (see Supporting Information of Schifani et al., 2019). The k_2' was fixed at 0.055 min^{-1} as determined by averaging the k_2 values found by SRTM in the temporal cortex, a large region with very low noise (Schifani et al., 2019). Instead of extracting the BP_{ND} from a voxel-based map as in the previous method, the BP_{ND} of each ROI for each participant was directly input into GAT using a Microsoft Excel spreadsheet.

2.6 | Network construction: Edge and node definition

We used a graph theory approach to examine the topological features of the dopamine D2R network using the structural morphometry package on the GAT (version 1.41) for MATLAB (R2014a)

(Figure 2). In the D2R network, nodes represent cortical regions of interest (ROI) as defined by the single-subject AAL brain atlas (Tzourio-Mazoyer et al., 2002). Two dopaminergic networks were examined: (a) 16 bilateral cortical ROIs (8 for each hemisphere) for the meso-cortical dopaminergic network (Figure 3a), and (b) 30 bilateral cortical ROIs (15 for each hemisphere) for the meso-limbic dopaminergic network (Figure 3b) These ROIs (ROIs listed in Tables 2 and 3) were delineated based on stereotaxic space (AAL single-subject atlas in MNI space). The networks were constructed based on the ROI division into two dopaminergic sub-networks found in Caminiti, Tettamanti, et al. (2017) (and used by Sala et al., 2017 to study early PD pathology) with modifications to remove the non-cortical ROIs and adding ROIs with evidence of D2R network involvement. To the meso-cortical network, we added the 1) inferior frontal gyrus pars triangularis (L/R) (Slifstein et al., 2015; Zakiniaeiz et al., 2019) because it forms part of the dorsolateral prefrontal cortex which is innervated by dopamine and involved in executive function; and to the meso-limbic network, we added the (a) medial cingulate cortex (L/R), (b) posterior cingulate cortex (L/R) (Nagano-Saito et al., 2017), (c) hippocampus (L/R) (Nyberg et al., 2016), (d) middle temporal pole (L/R), (e) superior temporal pole (L/R) (Wang et al., 1996; Werhahn et al., 2006), and (f) insula (L/R) (Christopher et al., 2014) which all have evidence of being part of the limbic system and have dopaminergic involvement.

In PET graph theory, unlike in fMRI, each participant has a single outcome brain image (e.g., binding potential, volume of distribution) from each scan session. For graph theory analysis, participants must be pooled together into groups to form group-level correlation matrices. Edges were represented by the linear correlation between D2R density as measured by the BP_{ND} of every pair of nodes as quantified by a Pearson correlation coefficient. A group-level BP_{ND} image was constructed for each of the three participant groups: HC, PD-CU, and PD-MCI. Interregional correlation matrices were calculated across participants for each group. Edges in each group's correlation matrix indicate how much D2R density in one ROI correlates to D2R density in another ROI across individuals (i.e., ROI with similar strength of BP_{ND}). The constructed group matrices of the meso-cortical dopaminergic network and the meso-limbic dopaminergic network are depicted in Figures 4a and 5a, respectively.

Using GAT, first the BP_{ND} was extracted for each of the ROIs. In the PVEC method, this was done using PKIN kinetic modeling toolbox (version 3.8) using TACs derived from PNEURO (version 4.005). In the no-PVEC method, the normalized, averaged BP_{ND} image of each group was input into GAT, along with the delineated ROIs in MNI space, which GAT then used to extract the BP_{ND} of each ROI. We adapted the simple graph model which was used in previous studies with PET (Kim et al., 2019). Using the group level correlation matrices, we created unweighted and undirected binary adjacency matrices for a range of sparsity thresholds from minimum sparsity to 0.34, increasing in 0.01 stepwise intervals. Sparsity refers to the ratio between the number of actual edges in the graph compared to the total number of edges possible (Achard & Bullmore, 2007). The matrices were binarized wherein

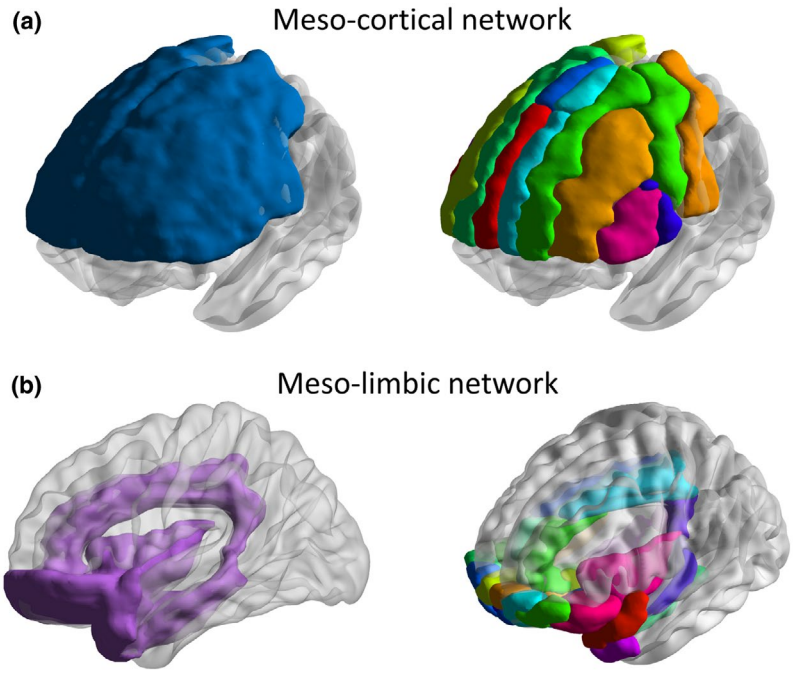

FIGURE 3 (a) The entire combined meso-cortical dopamine network (16 bilateral regions of interest) is shown in blue on the left and the corresponding multicolored individual regions of interest that comprise the blue cluster is show on the right. (b) The entire combined meso-limbic dopamine network (30 bilateral regions of interest) is shown in purple on the left and the corresponding multicolored individual regions of interest that comprise the purple cluster is show on the right. Multicolored individual regions of interest were included to aid the reader in visualizing the network. Brain networks were illustrated using BrainNet Viewer v1.7 (Xia et al., 2013). Tables 2 and 3 list the complete set of regions of interest used for the meso-cortical and meso-limbic networks, respectively [Color figure can be viewed at wileyonlinelibrary.com]

TABLE 2 Coordinates and abbreviations for the 16 meso-cortical dopamine network nodes of the automated anatomical labeling (AAL) atlas

Index	Regions (full name)	Abbreviations	MNI coordinates		
			X	Y	Z
1	Precentral gyrus	PRE.L	−39	−6	51
2		PRE.R	41	−8	52
3	Superior frontal gyrus	F1.L	−18	35	42
4		F1.R	22	31	44
5	Middle frontal gyrus	F2.L	−33	33	35
6		F2.R	38	33	34
7	Inferior frontal gyrus, opercular	F3OP.L	−48	13	19
8		F3OP.R	50	15	21
9	Inferior frontal gyrus, triangular	F3T.L	−46	30	14
10		F3T.R	50	30	14
11	Supplementary motor area	SMA.L	−5	5	61
12		SMA.R	9	0	62
13	Superior frontal gyrus, medial	F1M.L	−5	49	31
14		F1M.R	9	51	30
15	Postcentral gyrus	POST.L	−42	−23	49
16		POST.R	41	−25	53

Abbreviations: L, left hemisphere; MNI, Montreal Neurological Institute coordinates; R, right hemisphere.

a 1 was assigned if an edge existed between two ROIs, or assigned a 0 otherwise, with 0.10 sparsity meaning only the top 10% strongest correlations are assigned a 1 in that matrix and 90% of cells in the matrix are assigned a 0. The minimum sparsity was 0.28 for the meso-cortical network and 0.22 for the meso-limbic network, both of which were found by GAT. These are the lowest sparsities in which all nodes were fully connected to each other in all three groups for each respective dopamine network, that is, it is possible to travel between any two nodes in the graph at that sparsity threshold. The sparsity value of 0.34 is accepted to be the likely maximum sparsity value for an efficient small-world brain network (Achard & Bullmore, 2007).

2.7 | Topological measures

Our analysis focused on the novel characterization of the D2R network topology and examined the integration, segregation, and hub properties of these networks. The ability for the brain to integrate information from distant brain regions was measured by the following metrics: (a) small-worldness (σ; a measure of how efficient a network is at transferring information), (b) global efficiency (E_G; the ability for the brain to integrate distant nodes together), and (c) path length (L; the average number of steps requires to travel between any two nodes in a network) (Achard & Bullmore, 2007). Small-worldness (σ) is calculated by comparing the L and C of a network to an equivalent randomly generated network such that $\sigma = (C/C_{rand})/(L/L_{rand})$ where C_{rand} and L_{rand} are the mean clustering coefficient and mean path length respectively of this equivalent randomly generated network. Brain networks that are highly efficient and integrated will minimize the communication distance between all nodes in the network; that is, the fewest number of jumps is needed to travel between any two nodes.

We also assessed the ability of the brain to segregate into densely interconnected groups of regions, measuring: (a) local efficiency (E_L; the measure of how well a node integrates information with its immediate neighboring nodes) (Watts & Strogatz, 1998), (b) clustering coefficient (C; the measure how densely nodes connect together to form clusters) (Latora & Marchiori, 2001), and (c) modularity and Louvain modularity (M and M_L; the ability for a network to divide into smaller subnetworks in which nodes are highly interconnected within these modules and sparsely connected with nodes outside the module) (Newman & Girvan, 2004). Local efficiency is defined as the inverse of the shortest average path length in a subgraph comprising of $node_i$ and its adjacent neighbors (Latora & Marchiori, 2001). Local efficiency is considered a measure of fault tolerance in a network as it characterizes how well information is exchanged by neighbors of $node_i$ if $node_i$ is removed (Achard & Bullmore, 2007).

Finally, hubs are a measure of brain regions that are most important to network integrity which is typically measured in two ways. Degree centrality (De_i) is a measure of a node's hubness by counting the number of direct connections with other nodes in the graph, with more connections meaning greater degree centrality. Betweenness centrality (Be_i) is a measure of centrality which considers a node's influence on the overall flow of information in the graph by means of having the most information flowing through the node even if the node has few direct connections (Freeman, 1978). Hubs were identified based on the area under curve (AUC) method implemented in GAT, thresholded from minimum sparsity (0.28 for meso-cortical and 0.22 for meso-limbic) to 0.34. The AUC tests for statistical significance by analyzing the topological curves for each network measure across the designated sparsity range. These curves represent the changes in a specific network measures for each group as a function of sparsity, that is, they are the definite integral of the graph measures. In this study we consider a node as a hub if its regional betweenness/degree centrality is two standard deviations higher than the mean network degree/betweenness centrality (Bassett et al., 2008).

2.8 | Statistical analyses

Statistical significance of any group differences in parametric demographic and clinical measurements between all three groups was

TABLE 3 Coordinates and abbreviations for the 30 bilateral meso-limbic dopamine network nodes of the automated anatomical labeling (AAL) atlas

			MNI coordinates		
Index	Regions (full name)	Abbreviations	X	Y	Z
1	Inferior frontal gyrus, orbital	F3O.L	−36	31	−12
2		F3O.R	41	32	−12
3	Olfactory cortex	OC.L	−8	15	−11
4		OC.R	10	16	−11
5	Superior frontal gyrus, medial orbital	F1MO.L	−5	54	−7
6		F1MO.R	8	52	−7
7	Gyrus rectus	GR.L	−5	37	−18
8		GR.R	8	36	−18
9	Middle frontal gyrus, orbital	F1O.L	−31	50	−10
10		F1O.R	33	53	−11
11	Superior frontal gyrus, orbital	F1S.L	−17	47	−13
12		F1S.R	18	48	−14
13	Anterior cingulate	CIA.L	−4	35	14
14		CIA.R	8	37	16
15	Midcingulate	CINM.L	−5	−15	42
16		CINM.R	8	−9	40
17	Posterior cingulate	CIP.L	−5	−43	25
18		CIP.R	7	−42	22
19	Hippocampus	HIPP.L	−25	−21	−10
20		HIPP.R	29	−20	−10
21	Parahippocampal gyrus	PARA.L	−21	−16	−21
22		PARA.R	25	−15	−20
23	Amygdala	AMYG.L	−23	−1	−17
24		AMYG.R	27	1	−18
25	Superior temporal pole	T1A.L	−40	15	−20
26		T1A.R	48	15	−17
27	Middle temporal pole	T2A.L	−36	15	−34
28		T2A.R	44	15	−32
29	Insula	INS.L	−35	7	3
30		INS.R	39	6	2

Abbreviations: L, left hemisphere; MNI, Montreal Neurological Institute coordinates; R, right hemisphere.

determined using a one-way analysis of variance (ANOVA) in SPSS (SPSS Statistics 21; IBM Corp. Armonk, NY, USA), a two-sample *t* test was used to compare PD-CU and PD-MCI groups, a chi-square to compare sex ratio differences between the three groups, a Fisher's exact test to compare sex ratio differences between PD-CU and PD-MCI, and a Kruskal–Wallis H test was used to compare PD-CU and PD-MCI for the rank-based Hoehn and Yahr scores.

For the topological analyses, a nonparametric permutation test was used to evaluate statistically significant group differences. For this method we used 5,000 randomizations with the 95th percentile confidence interval as the critical value for a one-tailed test (uncorrected $p < 0.05$). Rejecting the null hypothesis indicates that there is a perceived difference in the topological parameters between the two groups. Each randomization was created by sorting the participants of the analysis at random into in two new groups such that each group has the same number of participants as the originally tested groups. An association matrix is created for each of the 5,000 randomized groups. These binarized random matrices are then thresholded at the same sparsity levels as the original group, and network measures are calculated for each sparsity. The original group's network measures are compared against the distribution of the 5,000 randomizations to check for significance. We used 20 null networks for the purposes of normalizing the graph measurements, which were randomly generated networks with the same number of nodes, connections, and degree distribution as the input networks of interest.

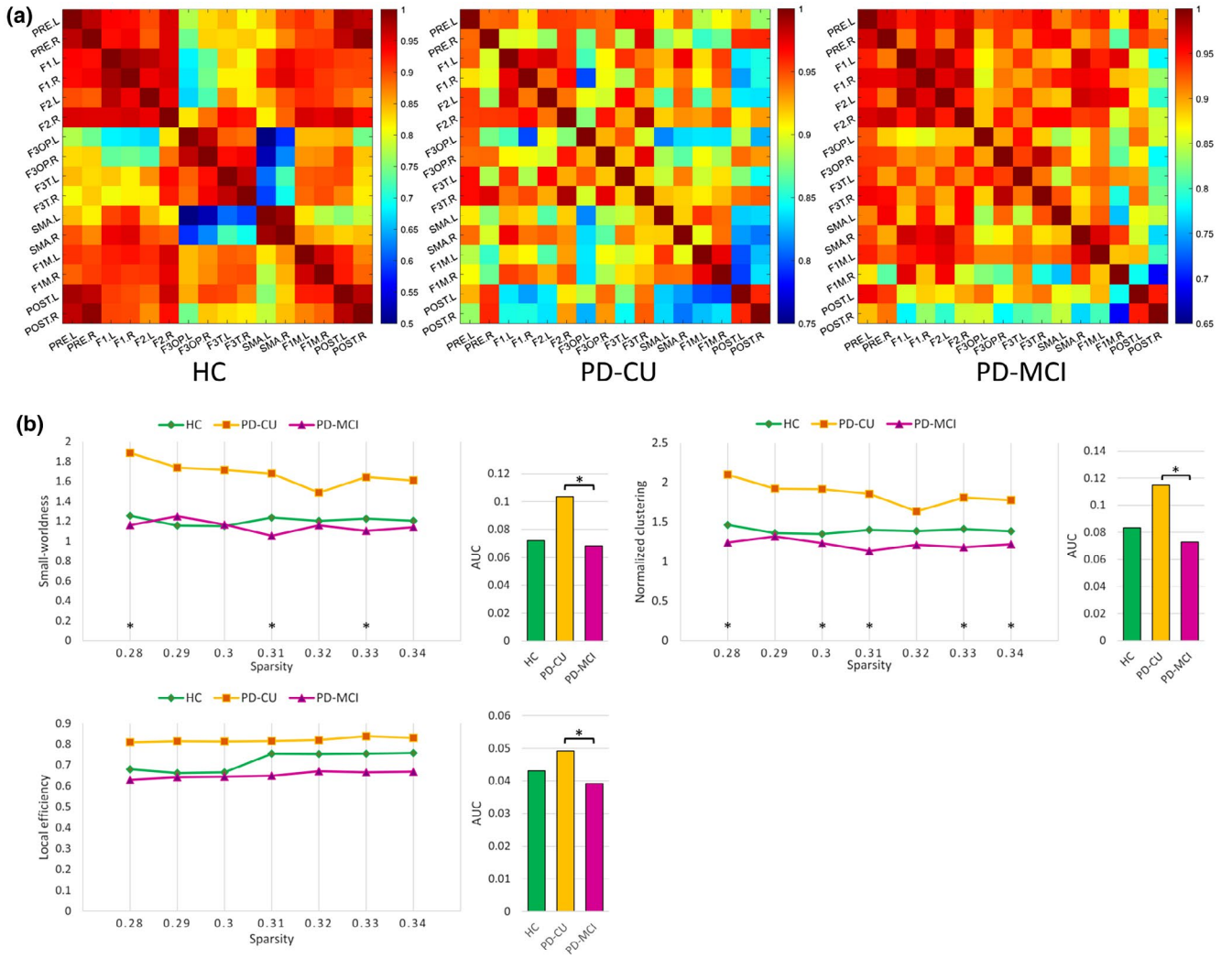

FIGURE 4 (a) Pearson correlation matrices for the three groups of healthy controls (HC), cognitively unimpaired Parkinson's disease patients (PD-CU), and Parkinson's disease patients with mild cognitive impairment (PD-MCI) shown for the 16 regions of interest of the meso-cortical dopamine network using the pre-processing method without partial volume effect correction. Table 2 lists the abbreviations used to label each matrix. The accompanying color bar represents the Pearson correlation coefficient values for the cells. (b) Line graphs showing the topological metric values of small-worldness, local efficiency, and normalized clustering as a function of sparsity ranging from 0.28 to 0.34 increasing stepwise by 0.01. Statistical significance was tested with a nonparametric permutation test using 5,000 randomizations. Asterisks on the line graphs denote a significant group difference was observed between the PD-CU and PD-MCI groups ($p < 0.05$) at that sparsity level using a 95% confidence interval. The bar graphs accompanying each line graph show the area under the curve (AUC) value for the respective line graph and an asterisk here signifies a statistically significant difference was found between PD-CU and PD-MCI groups for that topological measure ($p < 0.05$ uncorrected) [Color figure can be viewed at wileyonlinelibrary.com]

We tested the following three group comparisons: HC versus PD-CU, HC versus PD-MCI, and PD-CU versus PD-MCI. We applied AUC and functional density analysis (FDA) approaches found in GAT (Hosseini et al., 2012) to check for statistical significance across different sparsity levels and avoid the selection of a specific thresholding metric (Bassett & Bullmore, 2006; Bassett et al., 2012; Kim et al., 2019). Both the AUC metric and the FDA metric have been used in previous brain network studies for their utility in detecting topological differences in brain disorders (Kim et al., 2019; Zhang et al., 2011). FDA was additionally adopted due to the hypersensitivity of AUC at higher network sparsity which we observed in the D2R network (Bassett et al., 2012; Hosseini et al., 2012). Previous research has found that brain networks likely operate optimally with a small-world regime between 0.05 and 0.34 sparsity and so we limited our sparsity to within this range (Achard & Bullmore, 2007; Kim et al., 2019).

3 | RESULTS

3.1 | Demographics and clinical characteristics

Detailed demographic and clinical information of the 43 participants is shown in Table 1. The one-way between subjects ANOVA found

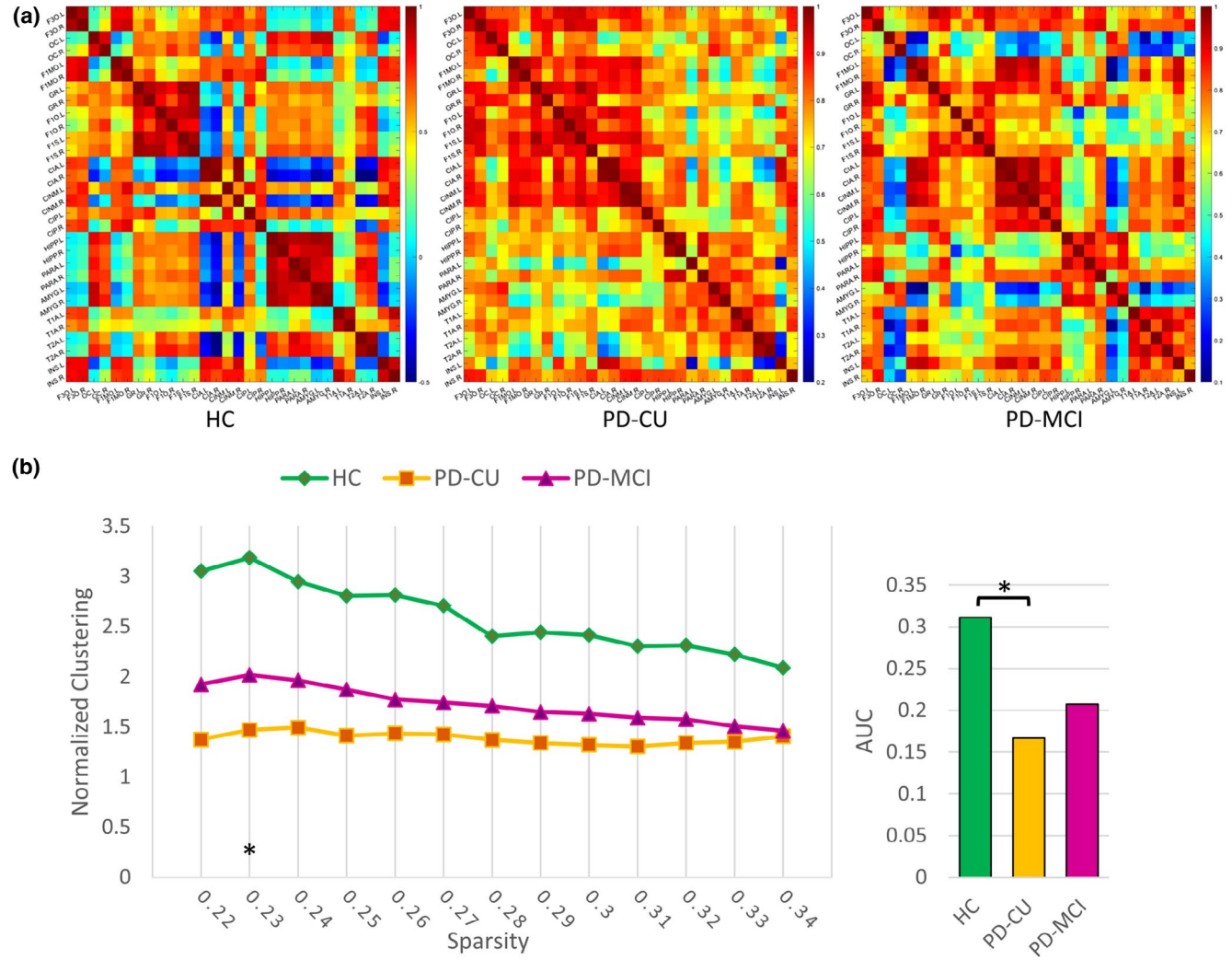

FIGURE 5 (a) Pearson correlation matrices for the three groups of healthy controls (HC), cognitively unimpaired Parkinson's disease patients (PD-CU), and Parkinson's disease patients with mild cognitive impairment (PD-MCI) shown for the 30 regions of interest of the mesolimbic dopamine network using the pre-processing method without partial volume effect correction. Table 3 lists the abbreviations used to label each matrix. The accompanying color bar represents the Pearson correlation coefficient values for the cells. (b) Line graph showing the topological metric values of normalized clustering as a function of sparsity ranging from 0.22 to 0.34 increasing stepwise by 0.01. Statistical significance was tested with a nonparametric permutation test using 5,000 randomizations. The asterisk on the line graph denotes a significant group difference was observed between the HC and PD-CU groups ($p < 0.05$) at that sparsity level using a 95% confidence interval. The bar graph accompanying the line graph shows the area under the curve (AUC) value for the line graph and an asterisk here signifies a statistically significant difference was found between HC and PD-CU groups for normalized clustering ($p < 0.05$ uncorrected) [Color figure can be viewed at wileyonlinelibrary.com]

a significant difference in MoCA score between the three groups, $F_{2, 40} = 50.23$; $n = 43$; $p < 0.001$, with PD-MCI having a statistically significant lower MoCA than both HC ($n = 30$; $p < 0.001$; Tukey post-hoc test PD-MCI vs. HC) and PD-CU ($n = 30$; $p < 0.001$; Tukey post-hoc test PD-MCI vs. PD-CU), which is expected due to the lower MoCA scores of the PD-MCI patients. One-way between subjects ANOVA revealed there were no group differences in terms of age, $F_{2, 40} = 2.819$; $n = 43$; $p = 0.07$, years of education, $F_{2, 40} = 1.623$; $n = 43$; $p = 0.21$, or depression score, $F_{2, 40} = 2.208$; $n = 43$; $p = 0.12$. There were no differences in terms of radioligand PET scan parameters between the three groups using a one-way between subjects ANOVA, with no difference found in injected doses, $F_{2, 40} = 0.941$; $n = 43$; $p = 0.40$, specific activity, $F_{2, 40} = 0.373$; $n = 43$; $p = 0.69$, and injected mass, $F_{2, 40} = 2.764$; $n = 43$; $p = 0.08$.

Comparing the PD-CU and PD-MCI groups using two-sample *t* test, the only difference between the two groups was found in MoCA score, $t_{24.39} = 7.48$; $n = 30$; $p < 0.001$. We did not find any group differences in terms of age, $t_{28} = -1.39$; $n = 30$, $p = 0.18$, years of education, $t_{28} = -0.48$; $n = 30$; $p = 0.64$, depression score, $t_{28} = 0.11$; $n = 30$; $p = 0.91$, disease duration, $t_{28} = 0.61$; $n = 30$; $p = 0.55$, UPDRS-III score, $t_{28} = -1.15$; $n = 30$; $p = 0.26$, or LEDD score, $t_{28} = 1.23$; $n = 30$; $p = 0.23$. A chi-square test showed a significant relationship between the three groups in terms of sex ratio ($X_2^2 = 7.35$; $n = 43$; $p = 0.03$). A Fisher's exact test comparing PD-CU and PD-MCI groups, however, found no significant sex differences between the two groups ($n = 30$; $p = 0.06$). The Fisher's exact test is useful for smaller sample sizes such as in this study while the chi-square test is sensitive to cells with small values (Jung, 2014). A

TABLE 4 Hubs of the three groups found using the no-PVEC methodology for each dopamine network. Degree and betweenness centrality values that are with an asterisk were found to be two standard deviations greater than the mean for that nodal measurement

Meso-cortical network	L/R	Be_i	De_i	Meso-limbic network	L/R	Be_i	De_i
Healthy controls				**Healthy controls**			
Middle frontal gyrus	R	6.44*	0.66*	Posterior cingulum	L	31.44*	1.02
PD-CU				**PD-CU**			
Middle frontal gyrus	R	3.44*	0.48	Amygdala	L	24.03*	0.38
				Olfactory bulb	R	28.14*	1.00
PD-MCI				**PD-MCI**			
Precentral	L	6.19*	0.60	Inferior frontal gyrus pars orbitalis	L	17.39*	1.67

Abbreviations: Be_i, betweenness centrality; De_i, degree centrality; L, left; PD-CU, cognitively unimpaired Parkinson's disease patients; PD-MCI, Parkinson's disease patients with mild cognitive impairment; R, right.

Kruskal–Wallis H test showed that there was no statistically significant difference in H&Y score between PD-MCI and PD-CU, $n = 30$; $p = 0.13$, with a mean rank H&Y score of 12.88 for PD-CU and 17.50 for PD-MCI.

3.2 | Dopaminergic network measurements no-PVEC

For the AUC and FDA analyses of the meso-cortical dopaminergic network, we found topological differences between the PD-CU group compared to the PD-MCI group (Figure 4b). Compared to PD-MCI for the sparsity range of 0.28 to 0.34. PD-CU had increased small-worldness ($p_{AUC} = 0.02$, $p_{FDA} = 0.02$), higher local efficiency ($p_{AUC} = 0.04$, $p_{FDA} = 0.03$), and higher normalized clustering ($p_{AUC} = 0.01$, $p_{FDA} = 0.02$). These p-values are all uncorrected and did not survive the false discovery rate (FDR) correction offered in GAT. We found no differences between the HC and either of the PD groups for the same sparsity values.

In the meso-limbic dopaminergic network analysis, we found significant group differences in the AUC and FDA between the PD-CU and the HC group for normalized clustering metric, but no differences were found between PD-CU and PD-MCI or between PD-MCI and HC groups (Figure 5b). Compared to HC for the sparsity range of 0.22 to 0.34, PD-CU had decreased normalized clustering ($p_{AUC} = 0.04$, $p_{FDA} = 0.04$).

3.3 | Dopaminergic network measurements with PVEC

When constructing the meso-cortical and meso-limbic D2R networks using the BP_{ND} images with PVEC, we found that a very high minimum sparsity was needed for all three-group comparisons in both dopamine networks (minimum sparsity > 0.34). Thus, no meaningful FDA and AUC analysis was possible as a result. To explain this observation, we investigated this in more detail and found that PVEC had two main effects. It increased the BP_{ND} on average for all three groups in both dopaminergic networks (Figure S1), and increased the variance as well, thus adding more noise to the graph theory analysis. There was no statistically significant interaction effect between PVEC/no-PVEC methodology and participant groups for the BP_{ND} using a two-way ANOVA (Figure S1), suggesting that PVEC uniformly increased BP_{ND} for all three participant groups, maintaining similar patterns of BP_{ND} overall for the three patient groups before and after PVEC (Figure S2).

3.4 | Hub organization

We also examined the hub organization of each group for the D2R networks. Table 4 lists all the hubs found in the no-PVEC preprocessing methodology based on nodal degree and betweenness centrality found using AUC network measures from minimum sparsity to 0.34. Hubs which were found for each group were depicted in Figure 6. In the meso-cortical network, the right middle frontal gyrus was found as a hub in both HC (both degree and betweenness centrality) and PD-CU (betweenness centrality) groups but was not found in the PD-MCI which instead had the left precentral gyrus as a betweenness hub. The meso-limbic network was characterized by different betweenness hubs for each of the three groups, with the left posterior cingulum found in HC, the left amygdala and right olfactory in the PD-CU and left inferior frontal orbital gyrus in PD-MCI. No degree centrality hubs were found in the meso-limbic network.

The PVEC method could not identify any meaningful hubs because graphs need to be fully connected to describe hub characteristics, and the minimum sparsity was too high (>0.34) for the PVEC methodology.

4 | DISCUSSION

In the present study, we investigated the extrastriatal dopaminergic subsystems in PD patients with and without cognitive impairment using a novel approach of analyzing the topological metrics of the extrastriatal D2R network measured through [^{11}C]FLB-457. Here we

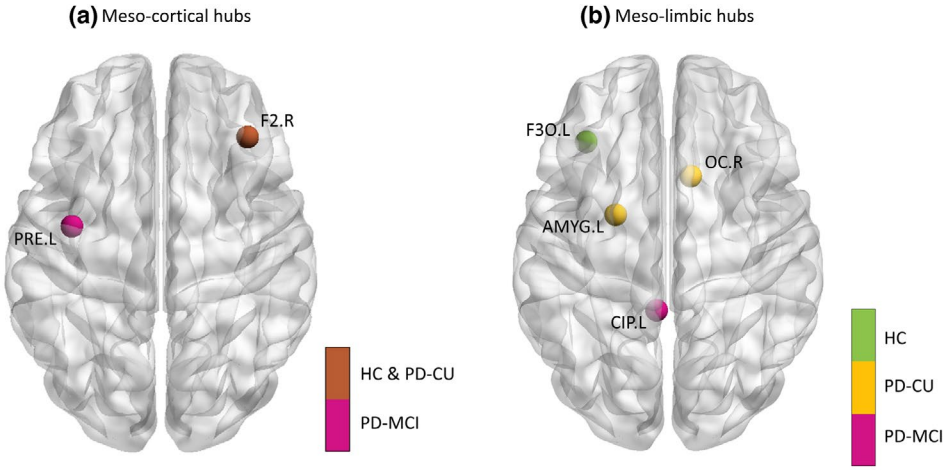

FIGURE 6 (a) Hub regions are shown for the healthy controls (HC), cognitively unimpaired Parkinson's disease patients (PD-CU), and Parkinson's disease patients with mild cognitive impairment (PD-MCI) groups for the 16 regions of interest (ROI) of the meso-cortical dopamine network and (b) the 30 ROIs of the meso-limbic dopamine network found using the pre-processing method without partial volume effect correction. Hubs were found by having two standard deviations greater degree centrality or betweenness centrality compared to the mean. We found two meso-cortical network hubs. The brown circle depicts the left precentral gyrus (PRE.L) region of interest (ROI) and was found in both the HC and PD-CU groups. This ROI was a betweenness centrality hub in both PD-CU and HC and a degree centrality hub in HC. The magenta circle depicts the right middle frontal gyrus ROI (F2.R) and was found in the PD-MCI group as a betweenness centrality hub. In the meso-limbic network we found four hubs. The green circle depicts the left posterior cingulum ROI (CIP.L) and was found in the HC group as a betweenness centrality hub. The yellow circles represent the left amygdala ROI (AMYG.L) and left olfactory bulb ROI (OC.R) which were both found in the PD-CU group as betweenness centrality hubs. The magenta circle depicts the left inferior frontal gyrus pars orbitalis ROI (F3O.L) and was found in the PD-MCI group as a betweenness centrality hub [Color figure can be viewed at wileyonlinelibrary.com]

presented both the methodological steps and results of preprocessing the imaging data using a parametric voxel-based method without employing PVEC and an ROI-based method with Müller–Gärtner PVEC approach applied, both parcellated using the AAL single-subject atlas. We found evidence that dysregulation of the meso-cortical dopamine network may be involved in cognitive decline in PD. In this network, we observed increased small-worldness, normalized clustering, and local efficiency in the PD-CU group compared to the PD-MCI group and a hub shift in the PD-MCI stage. Compensatory network reorganization likely occurs in this frontal dopamine network to preserve cognitive function in PD-CU patients. Other studies found the frontal and parietal regions to be especially vulnerable to hypometabolism in PD-MCI patients (Gonzalez-Redondo et al., 2014). The dopaminergic network appears to be heavily involved in the pathophysiology of cognitive decline in PD, with nigrostriatal and meso-cortical dopamine innervation being highly involved in executive function (Gratwicke et al., 2015). PVEC proved to be ineffective in conjunction with our graph theory analysis and we will discuss possible explanations why it failed.

This is the first study to examine the topological patterns of the D2R network in both HC participants and PD patients. Compared to PD-MCI, we found that the D2R network in the PD-CU group is characterized by altered topological architecture with an increase in local efficiency, normalized clustering, and small-worldness in the meso-cortical network, indicating perhaps a compensatory reorganization of the dopamine network may be involved in preserving the cognitive faculties of PD-CU patients. The meso-cortical dopamine network is likely involved in executive function (Gratwicke et al., 2015) with executive dysfunction being a key symptom of PD-MCI (Litvan et al., 2011). Preservation of functionality in this network despite disease pathology may account for why some PD-CU patients can maintain healthy cognitive function for long periods of time. Poston and colleagues (2016) found that PD patients maintain normal cognitive performance through compensatory hyperactivation of the putamen, with greater putamen activation leading to faster reaction time in a working memory/executive function task. The dorsal putamen is part of the meso-cortical dopamine network, but D2R cannot be measured in this brain region using [^{11}C]FLB-457. Using dynamic network-level topology, Shine and colleagues (2019) found that PD patients OFF medication had greater network-level integration than in the ON state, suggesting compensatory mechanisms occur when the PD symptoms are not being actively masked through treatment. These compensatory mechanisms may eventually fail with the increasing load of PD pathological degeneration leading to the emergence of cognitive complications.

The increased clustering and local efficiency found in the meso-cortical network for the PD-CU group compared to PD-MCI is likely capturing the network architecture changes that occur in PD-CU cognitive preservation. Increased local efficiency as a metric is thought to be responsible for making a network more fault tolerant and resistant to network attacks that remove a node. Utianski and colleagues (2016) found increased local clustering in PD-CU patients compared to HC using EEG, suggesting that PD-CU compensation may occur through emphasis on increased local connectivity. Isaacs

and colleagues (2019) proposed that PD-CU patients may be able to maintain their cognitive performance while performing a working memory task by increasing recruitment of both task-relevant fronto-striatal regions as well as novel regions beyond the task-related network. Taken together with these other findings, our results suggest PD-CU patients may be able to maintain normal cognition through network restructuring of the D2R meso-cortical network into a more inter-connected state. We hypothesize a possible inverted-U relationship in the meso-cortical dopaminergic network in terms of network efficiency, with PD-CU patients having a more integrated and efficient network than both HC and PD-MCI groups. An inverted-U relationship between cognitive performance and dopaminergic activity has been proposed for the basal ganglia and prefrontal cortices wherein too much or too little dopamine has a deleterious effect (Cools et al., 2001; Kroener et al., 2009; Williams & Goldman-Rakic, 1995). This inverted-U relationship in cognitive performance has also been observed with D2R activity specifically (Fresnoza et al., 2014; Papenberg et al., 2020). Monte-Silva and colleagues (2009) observed that both high and low doses of ropinirole, a D2/D3 dopamine agonist, impaired facilitatory neuroplasticity in the motor cortex, while the medium dose did not differ from the placebo. Mild cognitive impairment thus likely presents when the increasingly demanding progressive neurodegeneration in PD becomes too much for the compensatory mechanisms to handle and the meso-cortical network breaks down.

In the meso-limbic network topologies, we observed decreased normalized clustering in PD-CU compared to HC, but no differences between PD-MCI and HC or between PD-MCI and PD-CU. The limbic network has projections from the ventral tegmental area and is thought to be involved in memory, emotion, olfaction, and motivation which are heterogeneously affected by PD pathology (Bressan & Crippa 2005; Volkow et al., 2002). Sala and colleagues (2017) found no difference between HC and PD-CU patients in FDG-PET graph theory analysis of the meso-limbic dopaminergic network in terms of the number of connections between groups; only a difference in the meso-cortical network was found. The meso-cortical network has more easily observed and consistent network changes due to PD pathology suggesting a more reliable target for future investigation.

4.1 | PVEC analysis

We performed PVEC on our data set to test its effect on the topological results. Smith and colleagues (2019) found that PVEC increases BP_{ND} and reduces the effect of age and illness stage-related atrophy, but also increases the standard error, potentially leading to the introduction of more variance in the BP_{ND} estimation. The study concluded that PVEC may not be necessary if a high-resolution HRRT PET camera is employed and controlling for age-related volume loss is performed (Smith et al., 2019). A similar conclusion was reported by Uchida and colleagues (2011) which compared PVEC and no-PVEC BP_{ND} values of the serotonin 2A receptor as measured by an HRRT and found the BP_{ND} values to be consistent before and after PVEC. Importantly, the HRRT camera used by Uchida and colleagues (2011) is the same camera used by our study which was performed in the same PET center. When we applied PVEC, our study was not able to find any statistically significant results using the accepted FDA and AUC analysis methods. As noted beforehand, to explain our findings we investigated this in more detail and found that PVEC had two main effects. It did increase the BP_{ND} on average compared to the no-PVEC method, but it also increased the variance, in all three groups for the meso-cortical network, and for the PD-CU and PD-MCI groups in the meso-limbic network (see Table S1). The increased variance added more noise and probably acted as a confounding factor when analyzing the network topology. The weakest edges, those removed first when a lower percentage sparsity is applied, are the most affected by experimental noise, which may explain why the PVEC networks were only fully connected in a high sparsity threshold (>0.34) due to a prevalence of weak edges (Bordier et al., 2017). Furthermore, a global higher BP_{ND} is not necessarily better when using a Pearson correlation coefficient to create the adjacency matrices because GAT uses the relative relationships between values (Hosseini et al., 2012). If all the values in a matrix are uniformly doubled, the relationship between values remains the same. We analyzed the intraclass correlation coefficient (ICC) between the no-PVEC and PVEC BP_{ND} using a two-way mixed effects model checking for consistency between the two types of BP_{ND} for each participant in each brain region. The consistency measurement in the ICC measures the degree in which the two BP_{ND} values (PVEC and no-PVEC) equaled to each other plus a systemic error (i.e., $y = x + c$, c in this case being the consistent error created by lack of PVEC) (Koo & Li, 2016). We found the ICC values were very high between the two PET image processing methodologies, especially in the limbic and temporal cortices (see Figure S2). An ICC of 0.75 or higher is considered a good result of reliability between two measurements (Koo & Li, 2016) which we found for all brain regions in the average-measures ICC, which closely matches the pooling together of participants done in PET graph theory methodology. Overall, these observations seem to suggest that in certain situations the PVEC approach may add an additional confounding factor that must be taken into consideration.

4.2 | Hubs

Hubs are brain regions that are most important to the network architecture, either by having a lot of connections to other nodes (i.e., degree centrality) or by being a bridge for two other nodes to connect through (i.e., betweenness centrality) (Sporns et al., 2007). In the meso-cortical network, the right middle frontal gyrus was found as a hub in both HC and PD-CU patients but was not found in the PD-MCI group suggesting hub reorganization of the network occurs at this stage. The meso-cortical network was characterized by PD-CU having greater network efficiency than PD-MCI. The right middle frontal gyrus is a key area in the functional attentional network (Prell, 2018) and affected by atrophy in PD patients with

dementia (Nagano-Saito et al., 2005). The loss of this node's centrality may be a factor in PD-MCI conversion. The meso-limbic network was marked by shifting hubs in all three groups, changing from the left posterior cingulum in HC to the left amygdala and right olfactory in the PD-CU to left inferior frontal orbital gyrus in PD-MCI. The shifting of hubs in the three groups may be due to the heterogeneous nature of PD pathology and likely captures compensatory changes enacted by the brain to preserve DA brain network integrity in the face of PD disease progression. Sala and colleagues (2017) found no changes in the number of edges between HC and PD-CU in the meso-limbic network as measured by FDG-PET suggesting the changes we observed in the meso-limbic network occur due to masked dopaminergic dysregulation with otherwise spared brain function. Graph theory of specific neurotransmitter networks offers an adjuvant means of uncovering subtle brain changes that are otherwise difficult to observe.

4.3 | Future applications

This study shows the application of graph theory analysis to examine the network topology of neuroreceptor networks. Multivariate network analysis captures different aspects of the dopaminergic dysfunction compared to univariate regional comparisons of localized BP_{ND} differences. Subtle changes detected at the network level would otherwise be missed due to heterogeneity of the participant sample and the heterogeneity of PD etiology (Fazio et al., 2020). Using graph theory to quantify the topological measures of the brain is a valuable tool to the study of physiological underpinnings of other neurotransmitter systems both in a healthy and diseased state. AD subtypes were found to have distinct signatures in their network-level patterns that were associated with their structural atrophy patterns (Ferreira et al., 2019). There already exists much PET data that can be processed using our presented methodological pipelines to elucidate relationships that are hidden from univariate regional comparisons.

4.4 | Limitations

This study applied a methodological exploration of PET analysis and as such has some limitations that need to be considered. First, there were different results found in the D2R network using either PVEC or no-PVEC to process the [^{11}C]FLB-457 data. Graph theory analysis is very sensitive to changes in the input of data. The input that is being used (in our case the BP_{ND}) needs to be the gold standard for the radioligand that is being measured to be sure that findings are accurate. Another potential source of bias is in the choice of which ROIs to include in the analysis, which requires expertise in identifying ROIs with significant sources of the radioligand binding target and functional relevance to a network. Additionally, the present study only used the MoCA score to sort PD patients into either PD-CU and PD-MCI and a more comprehensive Level II MDS classification that can distinguish PD-MCI sub-types may benefit future studies. Another limitation is the small sample size which may also exacerbate the noise polluting the statistical and image data. Finally, [^{11}C]FLB-457 is not able to measure the BP_{ND} in the basal ganglia and so this region cannot be included as nodes in the network analysis. This study should be considered an exploratory study in PET graph theory methodology and further studies are necessary to confirm the results.

5 | CONCLUSIONS

Our results indicate that connective dysregulation of the extrastriatal dopamine network may be involved in cognitive decline in PD. We found that PD-CU patients have increased small-worldness, local efficiency, and normalized clustering compared to PD-MCI patients in the meso-cortical dopamine subnetwork, suggesting a compensatory reorganization of D2R architecture occurs at this stage of the disorder. Additionally, the PD-CU group had lower clustering in the meso-limbic dopaminergic subnetwork compared to the HC group. These findings suggest that extrastriatal dopaminergic connectivity patterns may play a role in the etiology of PD cognitive decline. Furthermore, these preliminary results demonstrate the utility in applying this graph theory analysis approach for other neuroreceptor systems and disease models in the future.

DECLARATION OF TRANSPARENCY

The authors, reviewers and editors affirm that in accordance to the policies set by the *Journal of Neuroscience Research*, this manuscript presents an accurate and transparent account of the study being reported and that all critical details describing the methods and results are present.

ACKNOWLEDGMENTS

The authors thank the staff of the Centre for Addiction and Mental Health Research Imaging Centre (Alvina Ng, Laura Nguyen and Anusha Ravichandran), Pablo Rusjan for his assistance in using the ROMI software and Eric Brown for his assistance in using the PNEURO software. This work was supported by Canadian Institutes of Health Research (CIHR) (MOP 136778). A.P.S. was supported by the Canada Research Chair program. A.M. was supported by the CIHR's Doctoral Award program.

CONFLICT OF INTEREST

The authors have no conflict of interest to declare.

AUTHOR CONTRIBUTIONS

Conceptualization, A.S.M., J.K., and A.P.S.; *Data Curation*, A.S.M., J.K., S.S.C., and L.C.; *Formal Analysis*, A.S.M. and J.K.; *Funding Acquisition*, A.S.M. and A.P.S.; *Investigation*, A.S.M., L.C., and Y.K.; *Methodology*, A.S.M. and J.K.; *Project Administration*, S.S.C.

and A.P.S.; *Resources*, L.C., Y.K., and A.P.S.; *Software*, A.S.M., J.K., A.G.G., and M.V.; *Supervision*, A.P.S., S.S.C., M.M., and A.G.G.; *Validation*, M.D.C.; *Visualization*, A.S.M.; *Writing – Original Draft*, A.M.; *Writing – Review & Editing*, A.S.M., J.K., M.M., A.G.G., M.V., M.D.C., Y.K., and A.P.S.

PEER REVIEW

The peer review history for this article is available at https://publons.com/publon/10.1002/jnr.24760.

DATA AVAILABILITY STATEMENT

The data that support the findings of this study are available on request from the corresponding author. The data are not publicly available due to privacy or ethical restrictions.

ORCID

Alexander S. Mihaescu https://orcid.org/0000-0002-8399-7883
Mikaeel Valli https://orcid.org/0000-0002-4059-2333

REFERENCES

Aarsland, D., Creese, B., Politis, M., Chaudhuri, K. R., Weintraub, D., & Ballard, C. (2017). Cognitive decline in Parkinson disease. *Nature Reviews Neurology*, *13*(4), 217.

Achard, S., & Bullmore, E. (2007). Efficiency and cost of economical brain functional networks. *PLoS Computational Biology*, *3*(2), e17.

Ashok, A. H., Myers, J., Marques, T. R., Rabiner, E. A., & Howes, O. D. (2019). Reduced mu opioid receptor availability in schizophrenia revealed with [11 C]-carfentanil positron emission tomographic Imaging. *Nature Communications*, *10*(1), 1–9.

Baggio, H. C., Sala-Llonch, R., Segura, B., Marti, M. J., Valldeoriola, F., Compta, Y., Tolosa, E., & Junqué, C. (2014). Functional brain networks and cognitive deficits in Parkinson's disease. *Human Brain Mapping*, *35*(9), 4620–4634.

Bassett, D. S., & Bullmore, E. D. (2006). Small-world brain networks. *The Neuroscientist*, *12*(6), 512–523.

Bassett, D. S., Bullmore, E., Verchinski, B. A., Mattay, V. S., Weinberger, D. R., & Meyer-Lindenberg, A. (2008). Hierarchical organization of human cortical networks in health and schizophrenia. *Journal of Neuroscience*, *28*(37), 9239–9248.

Bassett, D. S., Nelson, B. G., Mueller, B. A., Camchong, J., & Lim, K. O. (2012). Altered resting state complexity in schizophrenia. *NeuroImage*, *59*, 2196–2207.

Beck, A. T., Ward, C. H., Mendelson, M., Mock, J., & Erbaugh, J. (1961). An inventory for measuring depression. *Archives of General Psychiatry*, *4*(6), 561–571.

Bellucci, A., Mercuri, N. B., Venneri, A., Faustini, G., Longhena, F., Pizzi, M., Missale, C., & Spano, P. (2016). Parkinson's disease: From synaptic loss to connectome dysfunction. *Neuropathology and Applied Neurobiology*, *42*(1), 77–94.

Bordier, C., Nicolini, C., & Bifone, A. (2017). Graph analysis and modularity of brain functional connectivity networks: Searching for the optimal threshold. *Frontiers in Neuroscience*, *3*(11), 441.

Bressan, R. A., & Crippa, J. A. (2005). The role of dopamine in reward and pleasure behaviour—Review of data from preclinical research. *Acta Psychiatrica Scandinavica*, *111*, 14–21.

Bressler, S. L. (1995). Large-scale cortical networks and cognition. *Brain Research Reviews*, *20*(3), 288–304.

Bullmore, E., & Sporns, O. (2009). Complex brain networks: Graph theoretical analysis of structural and functional systems. *Nature Reviews Neuroscience*, *10*(3), 186–198.

Caminiti, S. P., Presotto, L., Baroncini, D., Garibotto, V., Moresco, R. M., Gianolli, L., Volonté, M. A., Antonini, A., & Perani, D. (2017). Axonal damage and loss of connectivity in nigrostriatal and mesolimbic dopamine pathways in early Parkinson's disease. *NeuroImage: Clinical*, *1*(14), 734–740.

Caminiti, S. P., Tettamanti, M., Sala, A., Presotto, L., Iannaccone, S., Cappa, S. F., Magnani, G., & Perani, D. (2017). Alzheimer's Disease Neuroimaging Initiative (ADNI). Metabolic connectomics targeting brain pathology in dementia with Lewy bodies. *Journal of Cerebral Blood Flow & Metabolism*, *37*(4), 1311–1325.

Chaudhuri, K. R., & Schapira, A. H. (2009). Non-motor symptoms of Parkinson's disease: Dopaminergic pathophysiology and treatment. *Lancet Neurology*, *8*(5), 464–474.

Christopher, L., Marras, C., Duff-Canning, S., Koshimori, Y., Chen, R., Boileau, I., Segura, B., Monchi, O., Lang, A. E., Rusjan, P., & Houle, S. (2014). Combined insular and striatal dopamine dysfunction are associated with executive deficits in Parkinson's disease with mild cognitive impairment. *Brain*, *137*(2), 565–575.

Chung, S. J., Yoo, H. S., Oh, J. S., Kim, J. S., Ye, B. S., Sohn, Y. H., & Lee, P. H. (2018). Effect of striatal dopamine depletion on cognition in de novo Parkinson's disease. *Parkinsonism & Related Disorders*, *1*(51), 43–48.

Cools, R., Barker, R. A., Sahakian, B. J., & Robbins, T. W. (2001). Enhanced or impaired cognitive function in Parkinson's disease as a function of dopaminergic medication and task demands. *Cerebral Cortex*, *11*(12), 1136–1143.

Cronin-Golomb, A. (2010). Parkinson's disease as a disconnection syndrome. *Neuropsychology Review*, *20*(2), 191–208.

Dalrymple-Alford, J. C., MacAskill, M. R., Nakas, C. T., Livingston, L., Graham, C., Crucian, G. P., Melzer, T. R., Kirwan, J., Keenan, R., Wells, S., & Porter, R. J. (2010). The MoCA: Well-suited screen for cognitive impairment in Parkinson disease. *Neurology*, *75*, 1717–1725.

De Lau, L. M., & Breteler, M. M. (2006). Epidemiology of Parkinson's disease. *Lancet Neurology*, *5*(6), 525–535.

Defer, G. L., Widner, H., Marié, R. M., Rémy, P., & Levivier, M. (1999). Core assessment program for surgical interventional therapies in Parkinson's disease (CAPSIT-PD). *Movement Disorders*, *14*(4), 572–584.

Díez-Cirarda, M., Strafella, A. P., Kim, J., Peña, J., Ojeda, N., Cabrera-Zubizarreta, A., & Ibarretxe-Bilbao, N. (2018). Dynamic functional connectivity in Parkinson's disease patients with mild cognitive impairment and normal cognition. *Neuroimage: Clinical*, *1*(17), 847–855.

Emre, M., Aarsland, D., Brown, R., Burn, D. J., Duyckaerts, C., Mizuno, Y., Broe, G. A., Cummings, J., Dickson, D. W., Gauthier, S., & Goldman, J. (2007). Clinical diagnostic criteria for dementia associated with Parkinson's disease. *Movement Disorders*, *22*(12), 1689–1707.

Evans, A. H., Katzenschlager, R., Paviour, D., O'Sullivan, J. D., Appel, S., Lawrence, A. D., & Lees, A. J. (2004). Punding in Parkinson's disease: Its relation to the dopamine dysregulation syndrome. *Movement Disorders*, *19*(4), 397–405.

Fazio, P., Ferreira, D., Svenningsson, P., Halldin, C., Farde, L., Westman, E., & Varrone, A. (2020). High-resolution PET imaging reveals subtle impairment of the serotonin transporter in an early non-depressed Parkinson's disease cohort. *European Journal of Nuclear Medicine and Molecular Imaging*, *47*(10), 2407–2416.

Ferreira, D., Pereira, J. B., Volpe, G., & Westman, E. (2019). Subtypes of Alzheimer's disease display distinct network abnormalities extending beyond their pattern of brain atrophy. *Frontiers in Neurology*, *10*, 524.

Floresco, S. B., & Magyar, O. (2006). Mesocortical dopamine modulation of executive functions: Beyond working memory. *Psychopharmacology*, *188*(4), 567–585.

Freeman, L. C. (1978). Centrality in social networks conceptual clarification. *Social Networks*, *1*(3), 215–239.

Fresnoza, S., Stiksrud, E., Klinker, F., Liebetanz, D., Paulus, W., Kuo, M. F., & Nitsche, M. A. (2014). Dosage-dependent effect of dopamine D2

receptor activation on motor cortex plasticity in humans. *Journal of Neuroscience*, *34*(32), 10701–10709.

Gill, D. J., Freshman, A., Blender, J. A., & Ravina, B. (2008). The Montreal cognitive assessment as a screening tool for cognitive impairment in Parkinson's disease. *Movement Disorders*, *23*(7), 1043–1046.

Goldman, J. G., & Litvan, I. (2011). Mild cognitive impairment in Parkinson's disease. *Minerva Medica*, *102*(6), 441.

Gonzalez-Redondo, R., García-García, D., Clavero, P., Gasca-Salas, C., García-Eulate, R., Zubieta, J. L., Arbizu, J., Obeso, J. A., & Rodríguez-Oroz, M. C. (2014). Grey matter hypometabolism and atrophy in Parkinson's disease with cognitive impairment: A two-step process. *Brain*, *137*(8), 2356–2367.

Göttlich, M., Münte, T. F., Heldmann, M., Kasten, M., Hagenah, J., & Krämer, U. M. (2013). Altered resting state brain networks in Parkinson's disease. *PLoS ONE*, *8*(10), e77336.

Gratwicke, J., Jahanshahi, M., & Foltynie, T. (2015). Parkinson's disease dementia: A neural networks perspective. *Brain*, *138*(6), 1454–1476.

Gunn, R. N., Lammertsma, A. A., Hume, S. P., & Cunningham, V. J. (1997). Parametric imaging of ligand-receptor binding in PET using a simplified reference region model. *NeuroImage*, *6*(4), 279–287.

Halldin, C., Farde, L., Högberg, T., Mohell, N., Hall, H., Suhara, T., Karlsson, P., Nakashima, Y., & Swahn, C. G. (1995). Carbon-11-FLB 457: A radioligand for extrastriatal D2 dopamine receptors. *Journal of Nuclear Medicine*, *36*(7), 1275–1281.

Hirsch, L., Jette, N., Frolkis, A., Steeves, T., & Pringsheim, T. (2016). The incidence of Parkinson's disease: A systematic review and meta-analysis. *Neuroepidemiology*, *46*(4), 292–300.

Hoops, S., Nazem, S., Siderowf, A. D., Duda, J. E., Xie, S. X., Stern, M. B., & Weintraub, D. (2009). Validity of the MoCA and MMSE in the detection of MCI and dementia in Parkinson disease. *Neurology*, *73*(21), 1738–1745.

Hosseini, S. H., Hoeft, F., & Kesler, S. R. (2012). GAT: A graph-theoretical analysis toolbox for analyzing between-group differences in large-scale structural and functional brain networks. *PLoS ONE*, *7*(7), e40709.

Isaacs, M. L., McMahon, K. L., Angwin, A. J., Crosson, B., & Copland, D. A. (2019). Functional correlates of strategy formation and verbal suppression in Parkinson's disease. *NeuroImage: Clinical*, *1*(22), 101683.

Ito, H., Sudo, Y., Suhara, T., Okubo, Y., Halldin, C., & Farde, L. (2001). Error analysis for quantification of [11C] FLB 457 binding to extrastriatal D2 dopamine receptors in the human brain. *NeuroImage*, *13*(3), 531–539.

Ito, K., Nagano-Saito, A., Kato, T., Arahata, Y., Nakamura, A., Kawasumi, Y., Hatano, K., Abe, Y., Yamada, T., Kachi, T., & Brooks, D. J. (2002). Striatal and extrastriatal dysfunction in Parkinson's disease with dementia: A 6-[18F] fluoro-l-dopa PET study. *Brain*, *125*(6), 1358–1365.

Jankovic, J. (2008). Parkinson's disease: Clinical features and diagnosis. *Journal of Neurology, Neurosurgery & Psychiatry*, *79*(4), 368–376.

Jokinen, P., Brück, A., Aalto, S., Forsback, S., Parkkola, R., & Rinne, J. O. (2009). Impaired cognitive performance in Parkinson's disease is related to caudate dopaminergic hypofunction and hippocampal atrophy. *Parkinsonism & Related Disorders*, *15*(2), 88–93.

Jung, S. H. (2014). Stratified Fisher's exact test and its sample size calculation. *Biometrical Journal*, *56*(1), 129–140.

Kim, J., Criaud, M., Cho, S. S., Díez-Cirarda, M., Mihaescu, A., Coakeley, S., Ghadery, C., Valli, M., Jacobs, M. F., Houle, S., & Strafella, A. P. (2017). Abnormal intrinsic brain functional network dynamics in Parkinson's disease. *Brain*, *140*(11), 2955–2967.

Kim, J., Ghadery, C., Cho, S. S., Mihaescu, A., Christopher, L., Valli, M., Houle, S., & Strafella, A. P. (2019). Network patterns of beta-amyloid deposition in Parkinson's disease. *Molecular Neurobiology*, *56*(11), 7731–7740.

Ko, J. H., Antonelli, F., Monchi, O., Ray, N., Rusjan, P., Houle, S., Lang, A. E., Christopher, L., & Strafella, A. P. (2013). Prefrontal dopaminergic receptor abnormalities and executive functions in Parkinson's disease. *Human Brain Mapping*, *34*(7), 1591–1604.

Koo, T. K., & Li, M. Y. (2016). A guideline of selecting and reporting intraclass correlation coefficients for reliability research. *Journal of Chiropractic Medicine*, *15*(2), 155–163.

Kroener, S., Chandler, L. J., Phillips, P. E., & Seamans, J. K. (2009). Dopamine modulates persistent synaptic activity and enhances the signal-to-noise ratio in the prefrontal cortex. *PLoS ONE*, *4*(8), e6507.

Lammertsma, A. A., & Hume, S. P. (1996). Simplified reference tissue model for PET receptor studies. *Neuroimage*, *4*(3), 153–158.

Latora, V., & Marchiori, M. (2001). Efficient behavior of small-world networks. *Physical Review Letters*, *87*(19), 198701.

Litvan, I., Aarsland, D., Adler, C. H., Goldman, J. G., Kulisevsky, J., Mollenhauer, B., Rodriguez-Oroz, M. C., Tröster, A. I., & Weintraub, D. (2011). MDS Task Force on mild cognitive impairment in Parkinson's disease: Critical review of PD-MCI. *Movement Disorders*, *26*(10), 1814–1824.

Litvan, I., Goldman, J. G., Tröster, A. I., Schmand, B. A., Weintraub, D., Petersen, R. C., Mollenhauer, B., Adler, C. H., Marder, K., Williams-Gray, C. H., Aarsland, D., Kulisevsky, J., Rodriguez-Oroz, M. C., Burn, D. J., Barker, R. A., & Emre, M. (2012). Diagnostic criteria for mild cognitive impairment in Parkinson's disease: Movement disorder society task force guidelines. *Movement Disorders*, *27*(3), 349–356.

Luo, C. Y., Guo, X. Y., Song, W., Chen, Q., Cao, B., Yang, J., Gong, Q. Y., & Shang, H. F. (2015). Functional connectome assessed using graph theory in drug-naive Parkinson's disease. *Journal of Neurology*, *262*(6), 1557–1567.

McCutcheon, R. A., Nour, M. M., Dahoun, T., Jauhar, S., Pepper, F., Expert, P., Veronese, M., Adams, R. A., Turkheimer, F., Mehta, M. A., & Howes, O. D. (2019). Mesolimbic dopamine function is related to salience network connectivity: An integrative positron emission tomography and magnetic resonance study. *Biological Psychiatry*, *85*(5), 368–378.

Monte-Silva, K., Kuo, M. F., Thirugnanasambandam, N., Liebetanz, D., Paulus, W., & Nitsche, M. A. (2009). Dose-dependent inverted U-shaped effect of dopamine (D2-like) receptor activation on focal and nonfocal plasticity in humans. *Journal of Neuroscience*, *29*(19), 6124–6131.

Morris, E. D., Chefer, S. I., Lane, M. A., Muzic, R. F., Jr., Wong, D. F., Dannals, R. F., Matochik, J. A., Bonab, A. A., Villemagne, V. L., Grant, S. J., & Ingram, D. K. (1999). Loss of D2 receptor binding with age in rhesus monkeys: Importance of correction for differences in striatal size. *Journal of Cerebral Blood Flow & Metabolism*, *19*(2), 218–229.

Müller-Gärtner, H. W., Links, J. M., Prince, J. L., Bryan, R. N., McVeigh, E., Leal, J. P., Davatzikos, C., & Frost, J. J. (1992). Measurement of radiotracer concentration in brain gray matter using positron emission tomography: MRI-based correction for partial volume effects. *Journal of Cerebral Blood Flow & Metabolism*, *12*(4), 571–583.

Nagano-Saito, A., Lissemore, J. I., Gravel, P., Leyton, M., Carbonell, F., & Benkelfat, C. (2017). Posterior dopamine D2/3 receptors and brain network functional connectivity. *Synapse*, *71*(11), e21993.

Nagano-Saito, A., Washimi, Y., Arahata, Y., Kachi, T., Lerch, J. P., Evans, A. C., Dagher, A., & Ito, K. (2005). Cerebral atrophy and its relation to cognitive impairment in Parkinson disease. *Neurology*, *64*(2), 224–229.

Narendran, R., Mason, N. S., Chen, C. M., Himes, M., Keating, P., May, M. A., Rabiner, E. A., Laruelle, M., Mathis, C. A., & Frankle, W. G. (2011). Evaluation of dopamine D2/3 specific binding in the cerebellum for the positron emission tomography radiotracer [11C] FLB 457: Implications for measuring cortical dopamine release. *Synapse*, *65*(10), 991–997.

Nasreddine, Z. S., Phillips, N. A., Bédirian, V., Charbonneau, S., Whitehead, V., Collin, I., Cummings, J. L., & Chertkow, H. (2005). The Montreal Cognitive Assessment, MoCA: A brief screening tool for mild cognitive impairment. *Journal of the American Geriatrics Society*, *53*(4), 695–699.

Newman, M. E., & Girvan, M. (2004). Finding and evaluating community structure in networks. *Physical Review E*, *69*(2), 026113.

Nyberg, L., Karalija, N., Salami, A., Andersson, M., Wåhlin, A., Kaboovand, N., Köhncke, Y., Axelsson, J., Rieckmann, A., Papenberg, G., & Garrett, D. D. (2016). Dopamine D2 receptor availability is linked to hippocampal–caudate functional connectivity and episodic memory. *Proceedings of the National Academy of Sciences of the United States of America*, *113*(28), 7918–7923.

Oades, R. D., & Halliday, G. M. (1987). Ventral tegmental (A10) system: Neurobiology. 1. Anatomy and connectivity. *Brain Research Reviews*, *12*, 117–165.

Olsson, H., Halldin, C., & Farde, L. (2004). Differentiation of extrastriatal dopamine D2 receptor density and affinity in the human brain using PET. *NeuroImage*, *22*(2), 794–803.

Papenberg, G., Karalija, N., Salami, A., Rieckmann, A., Andersson, M., Axelsson, J., Riklund, K., Lindenberger, U., Lövdén, M., Nyberg, L., & Bäckman, L. (2020). Balance between transmitter availability and dopamine D2 receptors in prefrontal cortex influences memory functioning. *Cerebral Cortex*, *30*(3), 989–1000.

Parkin, S. G., Gregory, R. P., Scott, R., Bain, P., Silburn, P., Hall, B., Boyle, R., Joint, C., & Aziz, T. Z. (2002). Unilateral and bilateral pallidotomy for idiopathic Parkinson's disease: A case series of 115 patients. *Movement Disorders*, *17*(4), 682–692.

Poston, K. L., YorkWilliams, S., Zhang, K., Cai, W., Everling, D., Tayim, F. M., Llanes, S., & Menon, V. (2016). Compensatory neural mechanisms in cognitively unimpaired Parkinson disease. *Annals of Neurology*, *79*(3), 448–463.

Prell, T. (2018). Structural and functional brain patterns of non-motor syndromes in Parkinson's disease. *Frontiers in Neurology*, *12*(9), 138.

Premi, E., Pilotto, A., Garibotto, V., Bigni, B., Turrone, R., Alberici, A., Cottini, E., Poli, L., Bianchi, M., Formenti, A., & Cosseddu, M. (2016). Impulse control disorder in PD: A lateralized monoaminergic frontostriatal disconnection syndrome? *Parkinsonism & Related Disorders*, *1*(30), 62–66.

Putcha, D., Ross, R. S., Cronin-Golomb, A., Janes, A. C., & Stern, C. E. (2015). Altered intrinsic functional coupling between core neurocognitive networks in Parkinson's disease. *NeuroImage: Clinical*, *1*(7), 449–455.

Rinne, J. O., Portin, R., Ruottinen, H., Nurmi, E., Bergman, J., Haaparanta, M., & Solin, O. (2000). Cognitive impairment and the brain dopaminergic system in Parkinson disease:[18F] fluorodopa positron emission tomographic study. *Archives of Neurology*, *57*(4), 470–475.

Rubinov, M., & Sporns, O. (2010). Complex network measures of brain connectivity: Uses and interpretations. *NeuroImage*, *52*(3), 1059–1069.

Rusjan, P., Mamo, D., Ginovart, N., Hussey, D., Vitcu, I., Yasuno, F., Tetsuya, S., Houle, S., & Kapur, S. (2006). An automated method for the extraction of regional data from PET images. *Psychiatry Research*, *147*(1), 79–89.

Sala, A., Caminiti, S. P., Presotto, L., Premi, E., Pilotto, A., Turrone, R., Cosseddu, M., Alberici, A., Paghera, B., Borroni, B., & Padovani, A. (2017). Altered brain metabolic connectivity at multiscale level in early Parkinson's disease. *Scientific Reports*, *7*(1), 1–2.

Sandiego, C. M., Gallezot, J. D., Lim, K., Ropchan, J., Lin, S. F., Gao, H., Morris, E. D., & Cosgrove, K. P. (2015). Reference region modeling approaches for amphetamine challenge studies with [11C] FLB 457 and PET. *Journal of Cerebral Blood Flow & Metabolism*, *35*(4), 623–629.

Schifani, C., Pruessner, J., Tseng, H. H., Rao, N., Tagore, A., Wilson, A. A., Houle, S., Rusjan, P. M., & Mizrahi, R. (2019). Stress-induced cortical dopamine response is altered in subjects at clinical high risk for psychosis using cannabis. *Addiction Biology*, *6*, e12812.

Seeman, P., & Madras, B.(Eds.). (2013). *Imaging of the human brain in health and disease*. Elsevier.

Shine, J. M., Bell, P. T., Matar, E., Poldrack, R. A., Lewis, S. J., Halliday, G. M., & O'Callaghan, C. (2019). Dopamine depletion alters macroscopic network dynamics in Parkinson's disease. *Brain*, *142*(4), 1024–1034.

Slifstein, M., Van De Giessen, E., Van Snellenberg, J., Thompson, J. L., Narendran, R., Gil, R., Hackett, E., Girgis, R., Ojeil, N., Moore, H., & D'Souza, D. (2015). Deficits in prefrontal cortical and extrastriatal dopamine release in schizophrenia: A positron emission tomographic functional magnetic resonance imaging study. *JAMA Psychiatry*, *72*(4), 316–324.

Smith, C. T., Crawford, J. L., Dang, L. C., Seaman, K. L., San Juan, M. D., Vijay, A., Katz, D. T., Matuskey, D., Cowan, R. L., Morris, E. D., & Zald, D. H. (2019). Partial-volume correction increases estimated dopamine D2-like receptor binding potential and reduces adult age differences. *Journal of Cerebral Blood Flow & Metabolism*, *39*(5), 822–833.

Sporns, O. (2011). The human connectome: A complex network. *Annals of the New York Academy of Sciences*, *1224*(1), 109–125.

Sporns, O., Honey, C. J., & Kötter, R. (2007). Identification and classification of hubs in brain networks. *PLoS ONE*, *2*(10), e1049.

Swerdlow, N. R. (Ed.). (2010). *Behavioral neurobiology of schizophrenia and its treatment*. Springer Science and Business Media.

Talairach, T., & Tournoux, P. (1988). *Co-planar stereotaxic atlas of the human brain*. Thieme Medical Publishers, Inc.

Telesford, Q. K., Joyce, K. E., Hayasaka, S., Burdette, J. H., & Laurienti, P. J. (2011). The ubiquity of small-world networks. *Brain Connectivity*, *1*(5), 367–375.

Tziortzi, A. C., Haber, S. N., Searle, G. E., Tsoumpas, C., Long, C. J., Shotbolt, P., Douaud, G., Jbabdi, S., Behrens, T. E., Rabiner, E. A., & Jenkinson, M. (2014). Connectivity-based functional analysis of dopamine release in the striatum using diffusion-weighted MRI and positron emission tomography. *Cerebral Cortex*, *24*, 1165–1177.

Tzourio-Mazoyer, N., Landeau, B., Papathanassiou, D., Crivello, F., Etard, O., Delcroix, N., Mazoyer, B., & Joliot, M. (2002). Automated anatomical labeling of activations in SPM using a macroscopic anatomical parcellation of the MNI MRI single-subject brain. *Neuroimage*, *15*(1), 273–289.

Uchida, H., Chow, T. W., Mamo, D. C., Kapur, S., Mulsant, B. H., Houle, S., Pollock, B. G., & Graff-Guerrero, A. (2011). Effects of aging on 5-HT2AR binding: A HRRT PET study with and without partial volume corrections. *International Journal of Geriatric Psychiatry*, *26*(12), 1300–1308.

Utianski, R. L., Caviness, J. N., van Straaten, E. C., Beach, T. G., Dugger, B. N., Shill, H. A., Driver-Dunckley, E. D., Sabbagh, M. N., Mehta, S., Adler, C. H., & Hentz, J. G. (2016). Graph theory network function in Parkinson's disease assessed with electroencephalography. *Clinical Neurophysiology*, *127*(5), 2228–2236.

Van Den Heuvel, M. P., & Pol, H. E. (2010 Aug 1). Exploring the brain network: A review on resting-state fMRI functional connectivity. *European Neuropsychopharmacology*, *20*(8), 519–534.

van Holstein, M., Aarts, E., van der Schaaf, M. E., Geurts, D. E., Verkes, R. J., Franke, B., van Schouwenburg, M. R., & Cools, R. (2011). Human cognitive flexibility depends on dopamine D2 receptor signaling. *Psychopharmacology*, *218*(3), 567–578.

Verger, A., Klesse, E., Chawki, M. B., Witjas, T., Azulay, J. P., Eusebio, A., & Guedj, E. (2018). Brain PET substrate of impulse control disorders in Parkinson's disease: A metabolic connectivity study. *Human Brain Mapping*, *39*(8), 3178–3186.

Veronese, M., Moro, L., Arcolin, M., Dipasquale, O., Rizzo, G., Expert, P., Khan, W., Fisher, P. M., Svarer, C., Bertoldo, A., & Howes, O. (2019). Covariance statistics and network analysis of brain PET imaging studies. *Scientific Reports*, *9*(1), 1–5.

Volkow, N. D., Fowler, J. S., Wang, G. J., & Goldstein, R. Z. (2002). Role of dopamine, the frontal cortex and memory circuits in drug addiction: Insight from imaging studies. *Neurobiology of Learning and Memory*, *78*(3), 610–624.

Volkow, N. D., Gur, R. C., Wang, G. J., Fowler, J. S., Moberg, P. J., Ding, Y. S., Hitzemann, R., Smith, G., & Logan, J. (1998). Association between decline in brain dopamine activity with age and cognitive and motor impairment in healthy individuals. *American Journal of Psychiatry*, *155*(3), 344–349.

Wang, G. J., Volkow, N. D., Fowler, J. S., Logan, J., Gur, R., Netusil, N., Hitzemann, R. J., & Pappas, N. S. (1996). Age associated decrements in dopamine D2 receptors in thalamus and in temporal insula of human subjects. *Life Sciences*, *59*(1), PL31–PL35.

Watts, D. J., & Strogatz, S. H. (1998). Collective dynamics of 'small-world' networks. *Nature*, *393*(6684), 440–442.

Wechsler, D. (1997). *Technical manual for the Wechsler adult intelligence and memory scale*. The Psychological Corporation.

Werhahn, K. J., Landvogt, C., Klimpe, S., Buchholz, H. G., Yakushev, I., Siessmeier, T., Müller-Forell, W., Piel, M., Rösch, F., Glaser, M., & Schreckenberger, M. (2006). Decreased dopamine D2/D3-receptor binding in temporal lobe epilepsy: An [18F] fallypride PET study. *Epilepsia*, *47*(8), 1392–1396.

Williams, G. V., & Goldman-Rakic, P. S. (1995). Modulation of memory fields by dopamine DI receptors in prefrontal cortex. *Nature*, *376*(6541), 572–575.

Woods, R. P., Mazziotta, J. C., & Cherry, S. R. (1993). MRI-PET registration with automated algorithm. *Journal of Computer Assisted Tomography*, *17*(4), 536–546.

Xia, M., Wang, J., & He, Y. (2013). BrainNet Viewer: A network visualization tool for human brain connectomics. *PLoS ONE*, *8*(7), e68910.

Zakiniaeiz, Y., Hillmer, A. T., Matuskey, D., Nabulsi, N., Ropchan, J., Mazure, C. M., Picciotto, M. R., Huang, Y., McKee, S. A., Morris, E. D., & Cosgrove, K. P. (2019). Sex differences in amphetamine-induced dopamine release in the dorsolateral prefrontal cortex of tobacco smokers. *Neuropsychopharmacology*, *44*(13), 2205–2211.

Zhang, J., Wang, J., Wu, Q., Kuang, W., Huang, X., He, Y., & Gong, Q. (2011). Disrupted brain connectivity networks in drug-naive, first-episode major depressive disorder. *Biological Psychiatry*, *70*(4), 334–342.

SUPPORTING INFORMATION

Additional Supporting Information may be found online in the Supporting Information section.

Transparent Peer Review Report

FIGURE S1 Two-way ANOVAs were conducted on six brain regions (left and right frontal and temporal cortices, bilateral insular cortex, and bilateral hippocampus) examining the effect of using or not using partial volume effect correction (PVEC) and group status of healthy controls (HC), cognitively unimpaired Parkinson's disease patients (PD-CU), and Parkinson's disease patients with mild cognitive impairment (PD-MCI) on non-displaceable binding potential. There was no statistically significant interaction between the effects of PVEC use and participant group on non-displaceable binding potential for any of the six brain regions. Left frontal cortex $F(2, 84) = 0.21$, $p = 0.81$; right frontal cortex $F(2, 84) = 0.26$, $p = 0.78$; left temporal $F(2, 84) = 0.04$, $p = 1.00$; right temporal $F(2, 84) = 0.22$, $p = 0.98$; bilateral insula $F(2, 84) = 0.01$, $p = 0.99$; bilateral hippocampus $F(2, 84) = 0.18$, $p = 0.84$

FIGURE S2 Intraclass correlation coefficients (ICC) of [^{11}C]FLB-457 non-displaceable binding potential (BP_{ND}) values using partial volume effect correction (PVEC) and without PVEC (no-PVEC) methodologies shown for the brain regions left and right frontal and temporal cortices, bilateral insular cortex and bilateral hippocampus. The ICC was calculated using a two-way mixed-effects model looking for consistency between the two differently calculated BP_{ND} for each participant labeled as a different colored line. Both the single measure ICC (comparing each pair of BP_{ND} values) and average measure ICC (averaging the BP_{ND} across each group) are labeled by each graph. Each colored line in these figures represents an individual participant's non-displaceable binding potential. 95% confidence intervals (CI-95%) are labeled next to each graph. The high ICC suggests that PVEC uniformly increased BP_{ND} for all three participant groups, maintaining similar pattern of BP_{ND} overall for the three patient groups with and without PVEC. An ICC of 0.75 or higher is considered a good result of reliability between two measurements

TABLE S1 Mean and variance binding potentials acquired both with and without partial volume effect correction (PVEC) for each participant group calculated for all ROIs in each network

TABLE S2 Intraclass correlation coefficients (ICC) of [^{11}C]FLB 457 non-displaceable binding potential (BP_{ND}) values using no-PVEC and PVEC methodologies shown for the brain regions left and right frontal and temporal cortices, bilateral insular cortex and bilateral hippocampus. The ICC was calculated using a two-way mixed-effects model looking for consistency between the two differently calculated BP_{ND} for each participant. Both the single measure ICC (comparing each pair of BP_{ND}) and average measure ICC (averaging the BP_{ND} across each group) presented, along with the respective 95% confidence intervals

Transparent Science Questionnaire for Authors

How to cite this article: Mihaescu, AS, Kim, J, Masellis, M, et al. Graph theory analysis of the dopamine D2 receptor network in Parkinson's disease patients with cognitive decline. *J Neurosci Res*. 2021;99:947–965. https://doi.org/10.1002/jnr.24760